國 立 交 通 大 學

光電工程研究所

碩 士 論 文

氧離子佈植與低溫成長砷化鎵光導天線在連續
波與脈衝波激發下產生兆赫波的研究

A comparative study of continuous-wave and pulsed terahertz
radiation generated by oxygen ion-implanted and
low-temperature-grown GaAs THz photoconductive antennas

研 究 生：楊孟桓

指導教授：潘犀靈　教授

鄔志偉　教授

中 華 民 國 九 十 七 年 七 月

氧離子佈植與低溫成長砷化鎵光導天線在連續波與脈衝波激發下
產生兆赫波的研究

A comparative study of continuous-wave and pulsed terahertz
radiation generated by oxygen ion-implanted and
low-temperature-grown GaAs THz photoconductive antennas

研 究 生：楊孟桓   Student：Mong-Huan Yang

指導教授: 潘犀靈　教授   Advisors：Prof. Ci-Ling Pan

鄒志偉　教授   Prof. Chi-Wai Chow

國 立 交 通 大 學
光 電 工 程 研 究 所
碩 士 論 文

A Thesis

Submitted to Institute of Electro-Optical Engineering

College of Electrical Engineering and Computer Science

National Chiao Tung University

In Partial Fulfillment of the Requirements

For the Degree of

Master of Engineering

In

Electro-Optical Engineering

July 2008

Hsinchu, Taiwan, Republic of China

中 華 民 國 九 十 七 年 七 月

氧離子佈植與低溫成長砷化鎵光導天線在連續波與脈衝波激發下產生兆赫波的研究

研究生：楊孟桓　　　　　　　　　　　　　指導教授：潘犀靈、鄒志偉 教授

國立交通大學光電工程研究所

摘 要

　　本論文討論在多重氧離子佈植砷化鎵 （ 2.5×10^{13} ions/cm^2 （500 keV & $800\,keV$）, 4×10^{13} ions/cm^2 (1200 keV) 薄膜材料及低溫成長之砷化鎵在脈衝波與連續波的激發下比較其兆赫波的特性。

　　多重氧離子佈值砷化鎵偶極天線在脈衝雷射與連續波雷射激發下都具有較高的兆赫波輻射功率，以 180mW 連續波雷射激發時多重氧離子佈植砷化鎵天線輻射功率 (2.27μW)大約比同結構的低溫成長砷化鎵（1.27μW）高。以 30mW 的脈衝光雷射激發時，多重氧離子佈植砷化鎵天線輻射功率(5.2mW)大約比同樣結構的低溫成長砷化鎵天線產生（3.6mW）高。另外多重氧離子佈值砷化鎵與低溫成長砷化鎵偶極天線在連續波與脈衝波激發下測量其頻寬皆可達 1THz。然而，低溫成長砷化鎵光導天線在連續波的激發下產生飽和的現象，多重氧離子佈值砷化鎵光導天線仍然沒有，因此多重氧離子佈值砷化鎵光導天線具有較好的兆赫波輸出功率。

A comparative study of continuous-wave and pulsed terahertz radiation generated by oxygen ion-implanted and low-temperature-grown GaAs THz photoconductive antennas

Student: Mong-Huan Yang

Advisors: Prof. Ci-Ling Pan
Prof. Chi-Wai Chow

Institute of Electro-Optical Engineering
College of Electrical Engineering and Computer Science
National Chiao Tung University

Abstract

THz wave was generated from dipole antenna-type devices made by using oxygen-ion implanted GaAs (GaAs:O) and low-temperature-grown GaAs (LT-GaAs). We compared the emission properties of LT-GaAs photoconductive (PC) antennas with GaAs:O fabricated condition（2.5×10^{13} ions/cm^2（$500\ keV\ \&\ 800\ keV$）, 4×10^{13} ions/cm^2（$1200\ keV$）in the pulse and CW mode. The absolute power of THz wave was also measured by a bolometer for comparison of the relative radiation power.

Compared GaAs:O with LT-GaAs at same structure of PC antennas. The material GaAs:O can generate higher THz power than LT-GaAs both in pulsed mode and CW mode. The THz power of GaAs:O (2.27μW) is higher than that of LT-GaAs(1.27μW) in CW mode, and in pulse mode, the THz peak amplitude of GaAs:O (5.2mW) is higher than that of LT-GaAs (3.6mW). The bandwidth of GaAs:O and LT-GaAs are measured about 1THz both under pulse (TDS) and CW (photomixing) pumping. However, the THz power of LT-GaAs is saturated on CW mode, while GaAs:O doesn't. The result shows that GaAs:O is a proper THz emitter compare with LT-GaAs which is hardly to reproduce.

Acknowledgement

致謝

    本論文得以順利的完成，首先要感謝指導老師潘犀靈教授及鄒志偉教授的悉心教導，提供良好的研究資源和實驗環境，讓我可以順利完成實驗。在這兩年研究生活中，我真的很感謝黎宇泰學長在實驗上的協助及理論的指導，使我獲益良多。也很感謝香港中文大學陳錦泰教授實驗室的陳克堅學長幫忙製作的光導天線和提供許多寶貴的意見及經驗。此外，也謝謝實驗室的王怡超、陳晉瑋學長們，及同學們：介暐、松輝、育賢因為有你們的陪伴，我的研究生生活才如此多采多姿，可以在枯燥的研究生活中帶來一些歡樂和喜悅，還有也謝謝學弟們：俞良、晏徵、承山、維駿、為弘幫忙處理實驗室的事務及在實驗器材的協助，也因為有你們的鼓勵及幫助，我才能順利畢業。

    最後，我要感謝我最親愛的家人：爸爸、媽媽和妹妹，在我求學過程中，一路上給予我最大的關懷與支持；陪伴我這幾年一路走來，給我的支持及鼓勵，讓我無後顧之憂，順利完成碩士學位！謝謝。

于新竹 交大

2008/08/22

Table of Contents

Table of Contents

List of Figures

List of Tables

Chapter 1   Introduction

1.1   Background

Terahertz range (wavelengths between 1000μm~300μm or frequencies between 300GHz~10THz) bridges the gap between microwave (mm-wave region) and infra-red frequencies, being until recently one of the least explored regions of the electromagnetic spectrum, which the frequency is near one trillion hertz (10^{12} Hz) as shown in Figure 1.1-1. Although terahertz radiation has already been researched in many fields in the past twenty years, wireless transmissions and computer clock speed are now at frequencies far below 1THz. THz radiation has been primarily developed for physicists and astronomers [01]. Based on heterodyne and Fourier transform techniques, these methods offered astronomers, chemists and space scientists a tool for investigating the thermal emission lines of
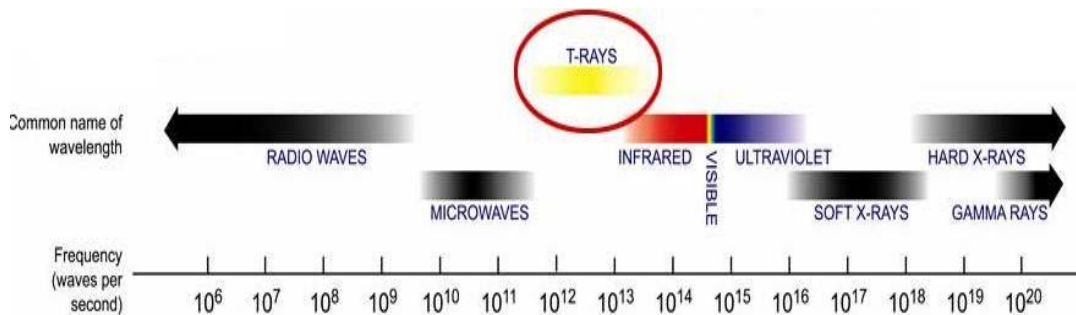
Figure 1.1-1 Electromagnetic spectrum.

(Refer to http://www.advancedphotonix.com/ap_products/terahertz_whatis.asp)

a wide diversity of light-weight molecules. The imaging technology and spectroscopic technology are studied in the Terahertz range [02]. Besides, it can be

applied not only to medical but also materials inspection. There is a great potential

for its application in many other scientific fields as well. In order to generate THz

radiation, femto-second pulse laser is the usual optical source, such as Ti-sapphire

laser, which is expensive and bulky. Using semiconductor laser diode can also

generate the continuous wave THz radiation. Coherent, tunable continuous-wave

(CW) THz sources are strongly needed in many applications such as

high-resolution spectroscopy, heterodyne receiver systems, local area networks

and so on.[03]

1.2 Method of generating THz radiation

Because of the resent development of pico-second and femto-second laser

system, there are various ways to generate the ultrashort pulsed millimeter and

submillimeter radiation [06], such as optical rectification and resonant THz

radiation in photoconductor generated by a pulse laser or optical heterodyne

downconversion occurs by illuminating the photomixer with two mode CW laser

beam.

1.2-1 Optical rectification

Using second ordered nonlinear effect of nonlinear crystal is one of methods

to generation THz. In this electro-optic medium, the low frequency electric field is

produced under intense optical illumination. The nonlinear optical process was

first suggested by Chung. [05] Optical rectification in a non-absorbing medium is

a process in which a laser pulse creates a time-dependent polarization that radiates an electric field which can be written as $\vec{E}(t) \propto \dfrac{\partial^2 \vec{P}}{\partial t^2}$ in the far field, where the polarization P follows the pulse intensity envelope. It is called rectification because the rapid oscillations of the electric field of the pulse laser are "rectified" and only the envelope of the oscillations remains. The schematic of the THz generation using optical rectification is shown in Figure 1.2-1. Since the medium is nonabsorbing, the polarization instantaneously follows the pulse envelope, and there is practically no limit on the speed at which the polarization can be switched on and off. The incident of polarization wave radiates a transient electric field which consists of one or one-and-a-half oscillation and therefore has a broadband THz frequency bandwidth. Bandwidth as large as 30 THz has been obtained using this generation mechanism.
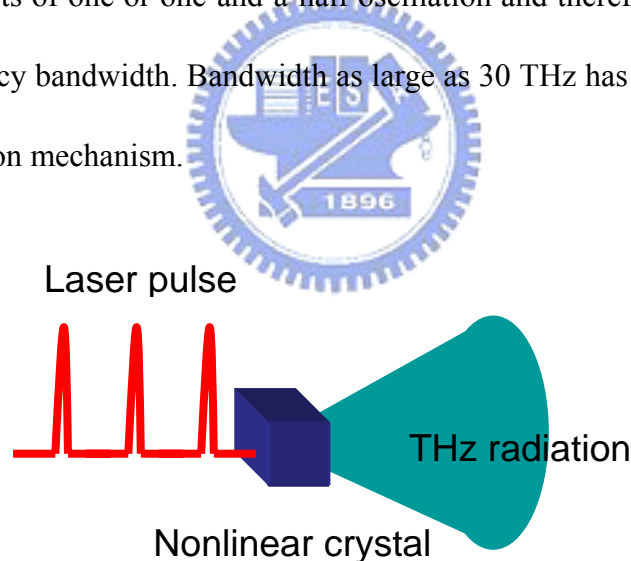
Figure 1.2-1 Optical rectification

1.2-2   Photoconductive switch

Biased PC switch can be used to generate THz radiation. It is generally based on the "current surge model" [06] which will be discussed in detail in the

next chapter. According to this model, as the energy of the input laser is higher than the energy of bandgap of photoconductor, then electron-hole pairs are excited and the mechanism to generated THz radiation can occur. Semiconductor such as GaAs (E_g=1.43eV), with the surface bands of a semiconductor lie within the energy produced by input photon and thus Fermi-level pinning occurs, leading to band bending and formation of a depletion region.

In briefly, the electromagnetic field of THz radiation is generated from a transient current which is generated on the surface of the photoconductor. Carriers are generated by the pulse laser instantaneously. In order to accelerate the carriers we add bias across the PC antenna. Then, the resultant transient current, or called current surge, produces an electric field on the surface of the photoconductor. This surface electric field is regarded as the source of the THz radiation. Figure 1.2-2 shows the setup for this method.
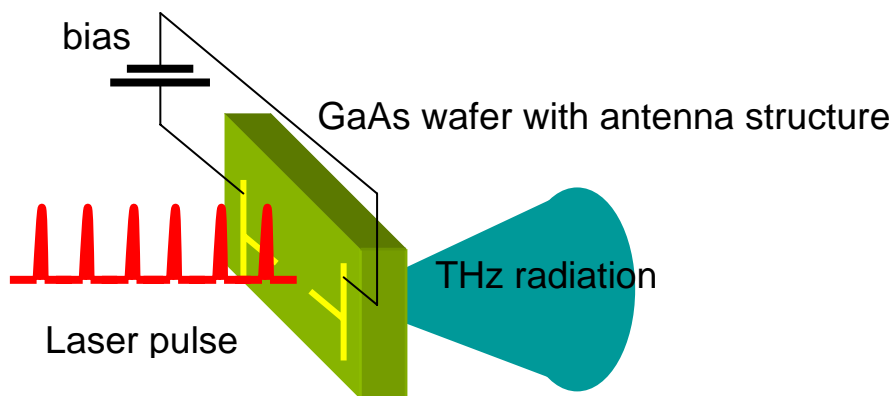
Figure 1.2-2 Photoconductive switch

1.2-3 Down-conversion from optical regime

Recently, CW Terahertz wave generation techniques have significant

developed. Using offset-frequency-locked CW lasers focused onto a small area of an appropriate photoconductor can generate the carriers. The laser induced photocarriers and shorted the gap producing a photocurrent which is modulated at the laser difference frequency. This current is coupled to an RF circuit or antenna that couples out or radiates the terahertz energy. The resulting power is narrow-band, phase lockable, and readily tuned over the full terahertz band by slightly shifting the optical frequency of one of the two lasers.

Different methods can be used to generation the CW THz wave, such as using one laser to generate two wavelengths by photomixing.[07-09], or using two independent lasers [10-11]. The advantages of using one laser include good spatial mode matching and high common-mode rejection ratio.

1.3   Method of detecting THz radiation

THz radiation is usually detected by liquid-helium cooled bolometer. There are different ways which are developed in recent years to detect THz radiation, such as photoconductive antenna and electro-optic sampling (EO sampling).

1.3-1   Liquid-helium cooled bolometer

Far-infrared (FIR), submillimeter wave and millimeter wave can be detected by Bolometer. A hot electron bolometer is a device, which absorbs the incident radiation to change the electron's temperature. Its resistance will respond for it

correspondingly. A traditional bolometer consists of a heat-sensitive detection element mounted inside a heat sink and physically supported by a thermally conductive physical supporter. The most common systems are helium-cooled Si, Ge and InSb bolometer. It can measure the radiation power lower in nanowatt region, but it losses the information of phase and frequency. Because of this, using bolometer to detect the power of THz radiation usually accompanies Martin-Puplett interferometer [12]. By using combined system, we can obtain the interferogram of THz radiation [13].

1.3-2 Photoconductive antenna

Using PC antenna as the detector is one of detecting THz radiation ways [14]. When the incident THz radiation illuminates the PC antenna, it induces transient current and then accelerate electron by probe beam. There are two factors determine the spectral bandwidth in this detector. One of them is the photocurrent response (i.e. carrier lifetime) and the other one is the frequency dependence of the antenna structure [15-16]. In general, the low frequency cutoff of the detectors results from the collection efficiency of the dipole, while the upper frequency limit is determined by the photocarrier response. The photocurrent response is the convolution of the optical pulse duration and the impulse current of the photoswitch across the photoconductive antenna on pulse mode.

1.3-3 Electro-Optical sampling

There are two advantages of Electro-Optical (EO) sampling, one is broad bandwidth spectrum and the other is easy to implement. Recently, technique of EO sampling has become an alternative to photoconductive (PC) detection [17]. The Zinc-Blende crystal was used to measure THz radiation based on the Pockels effect [17]. When we vary the temporal delay between pump and probe beam, the synchronous probe beam will probe the transient change of refractive index result from THz radiation changing the refractive index. There is a trade-off in this method, thick crystal will introduce longer interaction length but reduce the frequency response.

1.4 Material of Photoconductor antenna
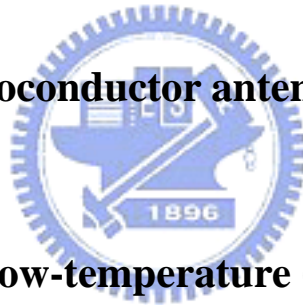
1.4-1 Material of Low-temperature (LT) grown GaAs

We often use LT-GaAs as the PC substrate. We use it for generation and detection of THz radiation because of the high resistivity ($10^7 \Omega cm$) [25] and good mobility (100-300 cm^2/Vs) [19-20], and short carrier lifetime ($<1ps$) [21-22]. But LT-GaAs has some drawback. One of them is the consistency of reproducing the sample. The quality of the material depends critically on both the growth temperature and the post growth thermal annealing conditions. An alternative material was reported to be promising as the substrate material of PC antennas, which is the arsenic ion-implanted GaAs [23]. These materials exhibit good structural and electrical properties and show ultrafast optoelectronic response. It is

possible to improve the carrier mobility of these ion-bombarded materials using post implantation thermal annealing process. Good control over the overall fabrication process allows studies of the influence of parameters such as the ion-implantation dose, the ion energy, and the thermal annealing conditions on the PC antenna characteristics.

1.4-2   Material of ion-implanted GaAs
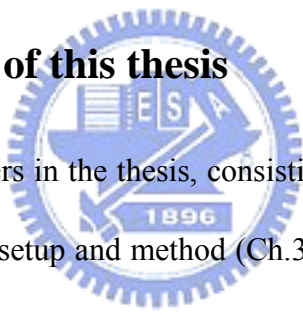
Many studies show that the arsenic (As) ion implanted GaAs PC antennas has better THz performance than those made on semi-insulating (SI) GaAs substrates [24-27]. It has been demonstrated that the terahertz emission property of arsenic ion-implanted GaAs has almost the same characteristics with the LT-GaAs. Such enhancement results from ultrafast carrier recombination associated with the presence of the implantation-induced defects. On the other hand, several groups have shown good characteristics of THz emitters when these devices are photoexcited near the anode with the use of PC antennas made on GaAs substrates grown by the Czochralski method. Although defects seem to play a crucial role in the characteristics of THz PC antenna emitters, there are very few studies that investigate the role of defects on these characteristics. Ion-implantation using other types of ions has already been used successfully to reduce the carrier lifetime in GaAs. For example, subpico-second lifetime can be obtained in GaAs:H GaAs:N and GaAs:O [28-33].

1.5 Objective

1.5-1 Motive

In this thesis, we used two different pumping source (pulse and CW) to measure the characteristics of the terahertz emitter fabricated on the substrates of GaAs:O and LT-GaAs. We compared the emission properties of GaAs:O PC antennas with LT-GaAs under different bias and pump power conditions. We also compare their spectra under different conditions.

1.5-2 Organization of this thesis

There are five chapters in the thesis, consisting of introduction (Ch.1), basic theory (Ch.2), experiment setup and method (Ch.3) result and analysis (Ch.4) and conclusion (Ch.5).

In chapter 1, we introduce the background of THz radiation and describe the motivation of the researching work. The basic theories about THz radiation generated from dipole antenna are mentioned in chapter 2 both on pulse and CW mode. The experiment setup and sample preparation are described in chapter 3. And in chapter 4, the results are analyzed and discussed. Finally, we will give a summary of the research work and list some future work in chapter 5.

Chapter 2　Basic Theory

In this chapter, we will explain the basic theory of using PC antenna to generate and detect THz radiation. And then, we will introduce the properties of material which is the substrates of the PC antennas.
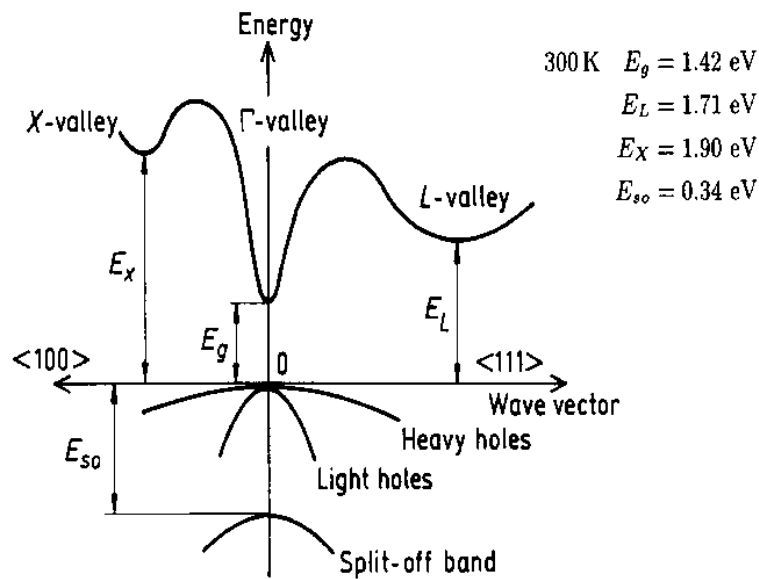
Figure 2.1-1 Energy band structure of GaAs
(Refer to http://www.ioffe.rssi.ru/SVA/NSM/Semicond/GaAs/bandstr.html)

2.1　The theory of generated THz radiation

When the small PC gap is irradiated by a femtosecond laser pulse with energy excess above the band gap of the semiconductor, the carriers will be created in the conduction band and valence band. The energy band structure of GaAs has is shown in Figural 2.1-1. The instantaneous concentration of the electron and hole pairs is high enough to "short-out" the gap. Then, by biasing the

electrode of the PC antenna; the carriers generated by the incident wave can be accelerated. This process can be found and expressed in the current-surge model.

2.1-1　Current-surge model

The first step, there are some time-average parameters which we need to define the THz radiation [29].

Charge density $\Rightarrow \rho(x,y,z,t)$

Current density $\Rightarrow \vec{J}(x,y,z,t)$

Electric field intensity $\Rightarrow \vec{E}(x,y,z,t)$

Magnetic flux density $\Rightarrow \vec{B}(x,y,z,t)$

Then, it is necessary to construct Maxwell's equation for current-surge model. According to Maxwell's equation [28]:

$$\nabla \times \vec{E} = -\frac{\partial \vec{B}}{\partial t} \qquad \text{(Faraday's Law)} \tag{2.1-1}$$

$$\nabla \bullet \vec{E} = \frac{\rho}{\varepsilon} \qquad \text{(Gauss Law)} \tag{2.1-2}$$

$$\nabla \times \vec{H} = \vec{J} + \frac{\partial \vec{D}}{\partial t} \qquad \text{(Ampere's Law)} \tag{2.1-3}$$

$$\nabla \bullet \vec{B} = 0 \tag{2.1-4}$$

And we know

$$\vec{B} = \nabla \times \vec{A} \tag{2.1-5}$$

From Equation (2.1-1) and (2.1-5), we can obtain:

$$\nabla \times \vec{E} = -\frac{\partial \vec{B}}{\partial t} = -\frac{\partial}{\partial t}\left(\nabla \times \vec{A}\right) = \nabla \times \left(-\frac{\partial \vec{A}}{\partial t}\right) \qquad \Rightarrow \nabla \times \left(\vec{E} + \frac{\partial \vec{A}}{\partial t}\right) = 0 \tag{2.1-6}$$

Then, we set a non-vector value V and employ that $\nabla \times \nabla V = 0$ to substitute the

Equation (2.1-6).

$$-\nabla V = \vec{E} + \frac{\partial \vec{A}}{\partial t} \Rightarrow \vec{E} = -\nabla V - \frac{\partial \vec{A}}{\partial t} \tag{2.1-7}$$

From Equation (2.1-3) 、 (2.1-5) and $\vec{H} = \frac{\vec{B}}{\mu}$ 、 $\vec{D} = \varepsilon\vec{E}$,we obtain

$$\frac{\nabla\times\vec{B}}{\mu} = \vec{J} + \varepsilon\frac{\partial \vec{E}}{\partial t} \Rightarrow \nabla\times\left(\nabla\times\vec{A}\right) = \mu\left(\vec{J} + \varepsilon\frac{\partial \vec{E}}{\partial t}\right) \tag{2.1-8}$$

Substitute Equation (2.1-7) into Equation (2.1-8)

$$\nabla\times\left(\nabla\times\vec{A}\right) = \mu\left[\vec{J} + \varepsilon\frac{\partial}{\partial t}\left(-\nabla V - \frac{\partial \vec{A}}{\partial t}\right)\right]$$

$$\nabla\left(\nabla\bullet\vec{A}\right) - \nabla^2\vec{A} = \mu\vec{J} - \mu\varepsilon\nabla\frac{\partial V}{\partial t} - \mu\varepsilon\frac{\partial^2\vec{A}}{\partial t^2}$$

$$\Rightarrow \nabla^2\vec{A} - \mu\varepsilon\frac{\partial^2\vec{A}}{\partial t^2} = -\mu\vec{J} + \nabla\left(\nabla\bullet\vec{A} + \mu\varepsilon\frac{\partial V}{\partial t}\right) \tag{2.1-9}$$

From Equation (2.1-2) and $\vec{D} = \varepsilon\vec{E}$

$$\nabla\bullet\left(\varepsilon\vec{E}\right) = -\nabla\bullet\left[\varepsilon\left(\nabla V + \frac{\partial \vec{A}}{\partial t}\right)\right] = \rho$$

$$\Rightarrow \nabla^2 V + \frac{\partial}{\partial t}\left(\nabla\bullet\vec{A}\right) = -\frac{\rho}{\varepsilon} \tag{2.1-10}$$

Due to Lorentz gauge assumption $\nabla\bullet\vec{A} + \varepsilon\mu\frac{\partial}{\partial t}V = 0$, Equation (2.1-9) becomes as

$$\nabla^2\vec{A} - \mu\varepsilon\frac{\partial^2\vec{A}}{\partial t^2} = -\mu\vec{J} \tag{2.1-11}$$

And, Equation (2.1-10) can be written as

$$\nabla^2 V - \mu\varepsilon\frac{\partial^2 V}{\partial t^2} = -\frac{\rho}{\varepsilon} \tag{2.1-12}$$

Equation (2.1-11) and (2.1-12) are the two inhomogeneous wave equations written

in terms of $\vec{A}$ and V. The two wave equations are used to determine a functional

and time dependent of the radiated electric field in the far field.

From Equation (2.1-3), the continuity equation of the free carriers is obtained.

$$\nabla \bullet \left(\nabla \times \vec{H} \right) = \nabla \bullet \left(\vec{J} + \frac{\partial \vec{D}}{\partial t} \right) = \nabla \bullet \vec{J} + \frac{\partial \rho}{\partial t} = 0 \qquad (2.1\text{-}13)$$

In the fact, the current density of the photoconductor antenna which adds the bias is the transverse current, parallel the surface of the PC antenna and perpendicular the direction of propagation. So that

$$\nabla \bullet \vec{J} = 0 \qquad (2.1\text{-}14)$$

From Equation (2.1-13) and (2.1-14), we can deduce that the charge density does not vary with time and not contribute the time dependent radiated electric field. As the result, Equation (2.1-7) becomes

$$\vec{E}\left(\vec{r}, t \right) = -\frac{\partial}{\partial t} \vec{A}(t) \qquad (2.1\text{-}15)$$

The solution of the vector potential $\vec{A}$ in Equation (2.1-11) leads into the Equation (2.1-15) to express the time dependent radiated electric field $\vec{E}_{rad}\left(\vec{r}, t \right)$ at the displacement $\vec{r}$ from the center of the PC antenna.

$$\vec{E}_{rad}\left(\vec{r}, t \right) = -\frac{1}{4\pi\varepsilon_0 c^2} \frac{\partial}{\partial t} \int \frac{\vec{J}_s\left(\vec{r}', t - \frac{\left| \vec{r} - \vec{r}' \right|}{c} \right)}{\left| \vec{r} - \vec{r}' \right|} da' \qquad (2.1\text{-}16)$$

where ε_0 is the permittivity of free space, c is the speed of light in vacuum, $\vec{J}_s$ is the surface current of the PC antenna in the retarded time, and da' is the increment of surface area at the displacement $\vec{r}'$ from the center of the PC antenna. The integration is covered with whole the optically illuminated area of the PC antenna. In the far field,

$$\left|\vec{r}\text{-}\vec{r'}\right| = r\left(1\text{-}\frac{\hat{n}\bullet\vec{r'}}{r}\right) \approx r \qquad (2.1\text{-}17)$$

The gap between the electrodes of the PC antenna is assumed to be uniformly illuminated by the optical source. Therefore, the surface current $\vec{J}_s$ can be set as a constant in space. Then, the radiated electric field in Equation (2.1-16) can be written as

$$\vec{E}_{rad}(\vec{r},t) = \text{-}\frac{1}{4\pi\varepsilon_0 c^2}\frac{A}{r}\frac{\partial}{\partial t}\vec{J}_s\left(t\text{-}\frac{r}{c}\right) \qquad (2.1\text{-}18)$$

where A is the illuminated area of the PC antenna and $r=\sqrt{x^2+y^2+z^2}$ .We considered that the THz radiation is generated on Z axis (i.e. x = y = 0), and let $t \to t\text{-}\left(\dfrac{z}{c}\right)$. Thus, The Equation (2.1-18) can be written as

$$\vec{E}_{rad}(\vec{r},t) = \text{-}\frac{1}{4\pi\varepsilon_0 c^2}\frac{A}{z}\frac{\partial}{\partial t}\vec{J}_s(t) \qquad (2.1\text{-}19)$$

If we want to know the CW radiation power of the antenna, we can use a simpler equivalent circuit of the antenna shown in figure2.1-2. The equivalent circuit equation can be written as:

$$C\frac{dv(t)}{dt} = \frac{V_b-v}{Z} - G(t) \qquad (2.1\text{-}20)$$

Where $G(t)$ is the conductance, C is the capacitance, Z is the radiation impedance. Solve the equation (2.1-20), we can get:

$$P = \frac{R}{2}\eta_1\lambda_1\eta_2\lambda_2(\frac{e}{hc})^2\frac{P_1 P_2}{[1+(\Omega\tau)^2][1+(\Omega RC)^2]} \qquad (2.1\text{-}21)$$

where λ_1 and λ_2 are the wavelength of the two pump lasers, P_1 and P_2 are the respective pump power, η_1 and η_2 are the external quantum efficiencies, Ω is the difference frequency, τ is the photocarrier lifetime, R is the resistance of the THz load circuit, C is the photomixer capacitance, and e , h , c are

well-known physical constants.

Beside, we can know the equation (2.1-22) from surface current [29].

$$\vec{J}_s(t) = \frac{\sigma_s(t)\vec{E}_b}{\frac{\sigma_s(t)\eta_0}{1+n}+1} \tag{2.1-22}$$

where n is the refractive index of photoconductor antenna under the wavelength of μm. η_0 is the impedance in free space, and $\sigma_s(t)$ is the surface conductivity which is shown in the equation (2.1-23).

$$\sigma_s(t) \equiv \frac{e(1-R)}{\hbar w}\int_{-\infty}^{t} dt' m(t,t')I_{opt}(t')\exp[\frac{-(t-t')}{\tau_{car}}] \tag{2.1-23}$$

where e is the electric charge, R is the reflectivity of photoconductor antenna, $\hbar w$ is the photon energy, $m(t,t')$ is the time-dependent carrier mobility at time t from created carrier at time t', I_{opt} is the time-dependent of optical intensity, and τ_{car} is the carrier lifetime of excited carriers. For the present derivation, we assume that carrier mobility is a constant.

$$m(t,t') = m \tag{2.1-24}$$

And assume that the carrier lifetime is long enough, $\tau_{car} \rightarrow \infty$. A Gaussian intensity profile of the optical beam is assumed:

$$I_{opt}(t') = I_0 \exp(\frac{-t'^2}{\tau^2}) \tag{2.1-25}$$

From these assumptions, the surface conductivity becomes

$$\sigma_s(t) \equiv \frac{e(1-R)}{\hbar w}I_0 \int_{-\infty}^{t} dt' m\exp(\frac{-t'^2}{\tau^2}) \tag{2.1-26}$$

From the equation (2.1-20) and (2.1-24) lead to the equation (2.1-19).

$$\vec{E}_{rad}(\vec{r},t) = -\frac{1}{4\pi\varepsilon_0 c^2}\frac{A}{z}\frac{e(1-R)}{\hbar w}I_0 m\exp(\frac{-t^2}{\tau^2}) \times \left[1+\frac{\eta_0 e(1-R)I_0 m}{(n+1)\hbar w}\int_{-\infty}^{t/\tau}\tau\exp(-x^2)dx\right]^{-2} \tag{2.1-27}$$

Comparing with the result from experiment, it is necessary to rewrite the

-15-

equation (2.1-25) in term of the experimental parameters E_b which is the bias electric field applied across the photoconductor, and F_{opt} which is the incident optical intensity.

$$F_{opt} = \int_{-\infty}^{\infty} I_0 \exp(\frac{-t^2}{\tau^2})dt = \sqrt{\pi}I_0\tau \equiv \frac{E_{opt}}{A} \qquad (2.1\text{-}28)$$

Where E_{opt} is the average optical energy and A is the area of the incident optical beam. Then we define the parameter B and D to simplify the equation.

$$B = \frac{Ae(1-R)m}{4\pi\varepsilon_0 c^2 z\hbar w\sqrt{\pi}} \qquad (2.1\text{-}29)$$

$$D = \frac{\eta_0 e(1-R)m}{(n+1)\hbar w\sqrt{\pi}} \qquad (2.1\text{-}30)$$

And then, the electric field in the far field can be written as

$$E_{rad}(t) = -BE_b\frac{F_{opt}}{\tau}\exp(\frac{-t^2}{\tau^2})\times\left[1+DF_{opt}\int_{-\infty}^{t/\tau}\exp(-x^2)dx\right]^{-2} \qquad (2.1\text{-}31)$$

Beside of current surge model, we can also discuss on the point of the carrier dynamics in semiconductor to analyze the THz generation by Drude-Lorentz model when we need to discuss the factor of material in PC antenna [30-31].

2.1-2 Drude-Lorentz model

For the calculation of carrier transport and THz radiation in a biased semiconductor, the one-dimensional Drude-Lorentz model is used. When a biased semiconductor is pumped by a laser pulse with photon energies greater than the band gap of the semiconductor, electrons and holes will be created in the conduction band and valence band, respectively. The carrier pumped by ultrashort laser pulse is trapped in the mid-gap states with the time constant of the carrier

trapping time. The time-dependence of carrier density is given by the following equation.

$$\frac{dn(t)}{dt} = -\frac{n(t)}{\tau_c} + G(t) \qquad (2.1\text{-}32)$$

Where n(t) is the density of the carrier, G(t) is the generation rate of the carrier by the laser pulse, and τ_c is the carrier trapping time. The generated carriers will be accelerated by the bias electric field. The acceleration of electrons (holes) in the electric field is given by

$$\frac{d\nu_{e,h}(t)}{dt} = -\frac{\nu_{e,h}(t)}{\tau_s} + \frac{q_{e,h}}{m_{e,h}} E \qquad (2.1\text{-}33)$$

Where $\nu_{e,h}(t)$ is the average velocity of the carrier, $q_{e,h}$ is the charge of an electron (a hole), $m_{e,h}$ is the effective mass of the electron (hole), $\tau_{e,h}$ is the momentum relaxation time, and E is the local electric field. The subscript e and h represent electron and hole, respectively. The local electric field E is smaller than the applied bias electric field E_b due to the screening effects of the space charges,

$$E = E_b - \frac{P}{\alpha\varepsilon} \qquad (2.1\text{ -}34)$$

Where P is the polarization induced by the spatial separation of the electron and hole, ε is the dielectric constant of the substrate and α is the geometrical factor of the PC material. The geometrical factor α is equal to three for an isotropic dielectric material. It is noted that both, the free and trapped carriers contribute to the screening of the electric field. The time dependence of polarization P can be written as

$$\frac{dP}{dt} = -\frac{P}{\tau_r} + J \qquad (2.1\text{-}35)$$

Where τ_r is the recombination time between an electron and hole. In the equation (2.1-33), J is the density of the current contributed by an electron and hole,

$$J = en\nu_h - en\nu_e \qquad (2.1\text{-}36)$$

Where e is the charge of a proton. The change of electric currents leads to electromagnetic radiation according to Maxwell's equations. In a simple Hertzian dipole theory, the far-field of the radiation E_{THz} is given by

$$E_{THz} \propto \frac{\partial J}{\partial t} \qquad (2.1\text{-}37)$$

To simplify the following calculations, we introduce a relative speed ν between an electron and hole,

$$\nu = \nu_h - \nu_e \qquad (2.1\text{-}38)$$

Then the electric field of THz radiation can be expressed as

$$E_{THz} \propto e\nu \frac{\partial n}{\partial t} + en \frac{\partial \nu}{\partial t} \qquad (2.1\text{-}39)$$

The first term on the right hand side of the equation (2.1-37) represents the electromagnetic radiation due to the carrier density change, and the second term represents the electromagnetic radiation which is proportional the acceleration of the carrier under the electric field.

2.1-3 Photomixing

CW THz wave can be generated through photomixing which produces optical intensity beating at THz frequencies by mixing two single-mode lasers or mode beating within a single laser. The combination of two waves with slightly

different frequencies is equivalent to a wave which envelope is modulated by the difference frequency. The intensity-modulated beam will excite the electron-hole pairs in PC antennas then accelerated by the bias voltage applied to the PC antennas. The generated THz frequency is as the same as the optical beating frequency.

When two electric fields with slightly different frequencies propagate collinearly into biased PC antennas, beating signal will be radiated. Set two parallel, scalar electric fields as:

$$E_1(t) = E_{10}(t)Cos(w_1 t + \phi_1)$$
$$E_2(t) = E_{20}(t)Cos(w_2 t + \phi_2)$$

(2.1-40)

Where E_{10}, E_{20}, w_1, w_2, ϕ_1 and ϕ_2 are the amplitude, angular frequency and constant phases of wave 1 and wave 2, respectively. And the total electric filed is the superposition of the two waves:

$$E(t) = E_1(t) + E_2(t) = E_1 Cos(w_1 t + \phi_1) + E_2 Cos(w_2 t + \phi_2)$$

(2.1-41)

From the simulated curves of figure 2-1-2, we can see that the total electric field has the waveform with a slowly various envelope and a fast carrier frequency inside.
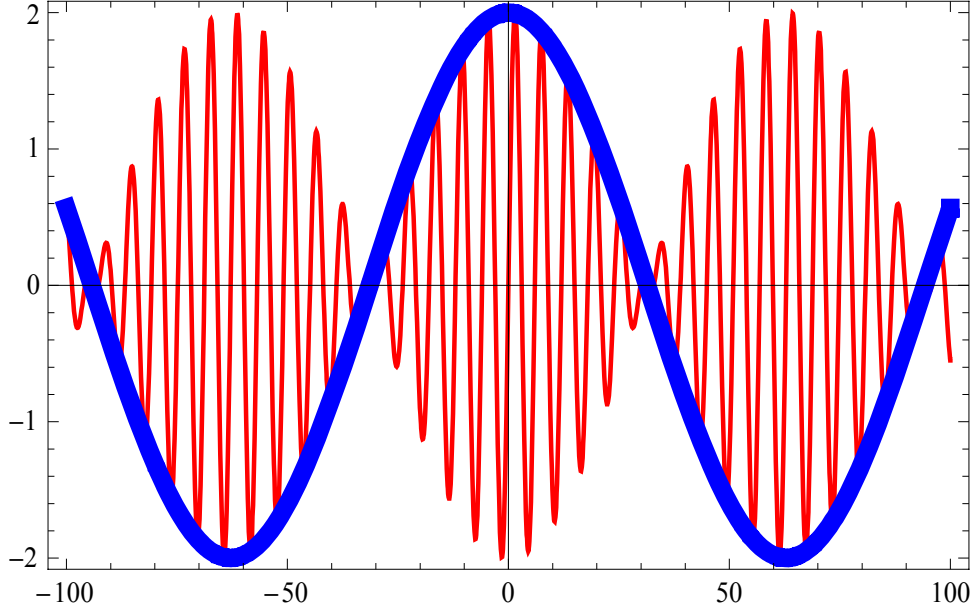
Figure 2.1-2 The simulated curves of two wave with slightly different frequencies. The thin curve is the sum of the two waves. The thick curve is the plot of the wave with frequency of (w_1 - w_2)/2

Because the PC antenna has photocarrier lifetime about 1 ps, so it can't response the faster frequencies. The beating intensity needs to be time averaged:

$$I_{beat}(t) = c\varepsilon_0 < E^2(t') >_T = c\varepsilon_0 \int_{-\frac{T}{2}}^{\frac{T}{2}} (E_1(t') + E_2(t'))^2 dt'$$

$$= c\varepsilon_0 \int_{-\frac{T}{2}}^{\frac{T}{2}} [E_1^2 Cos^2(w_1t'+\phi_1) + E_2^2 Cos^2(w_2t'+\phi_2) + 2E_1E_2Cos(w_1t'+\phi_1)Cos(w_2t'+\phi_2)]dt'$$

$$= \frac{c\varepsilon_0}{T} \int_{-\frac{T}{2}}^{\frac{T}{2}} \{E_1^2 \frac{1+Cos2(w_1t'+\phi_1)}{2} + E_2^2 \frac{1+Cos(w_2t'+\phi_2)}{2} +$$

$$E_1E_2Cos[(w_1t'+\phi_1)+(w_2t'+\phi_2)] + E_1E_2Cos[(w_1t'+\phi_1)+(w_2t'+\phi_2)]\}dt'$$

$$= \frac{c\varepsilon_0}{T} \{E_1^2[\frac{T}{2} + \frac{Sin2(w_1t'+\phi_1)}{2}\Big|_{t-\frac{T}{2}}^{t+\frac{T}{2}}] + E_2^2[\frac{T}{2} + \frac{Sin2(w_2t'+\phi_1)}{2}\Big|_{t-\frac{T}{2}}^{t+\frac{T}{2}}] +$$

$$E_1E_2 \frac{Sin[(w_1+w_2)t'+(\phi_1+\phi_2)]}{w_1+w_2}\Big|_{t-\frac{T}{2}}^{t+\frac{T}{2}} + E_1E_2 \frac{Sin[(w_1-w_2)t'+(\phi_1-\phi_2)]}{w_1-w_2}\Big|_{t-\frac{T}{2}}^{t+\frac{T}{2}}\}$$

$$(2.1\text{-}42)$$

where c is the speed of light in vacuum, ε_0 is the permittivity of free space, T

is the detector response time.

We know that

$$\frac{Sin(wt'+\phi)}{wT}\bigg|_{t-\frac{T}{2}}^{t+\frac{T}{2}} = \frac{Sin[w(t+\frac{T}{2})+\phi]-Sin[w(t-\frac{T}{2})+\phi]}{wT} = \frac{2Cos(wt+\phi)Sin(\frac{wT}{2})}{wT}$$

$$= Cos(wt+\phi)Sinc(\frac{wT}{2})$$

(2.1-43)

Where $Sinc(\frac{wT}{2}) = \dfrac{Sin(\frac{wT}{2})}{\frac{wT}{2}}$.

Substituing (2.1-25) into (2.1-24), the formula will become simpler:

$$I_{beat}(t) = c\varepsilon_0 \{\frac{E_1^{\,2}}{2} + E_1^{\,2}Cos(2w_1t+\phi_1)Sinc(w_1t)$$

$$+\frac{E_2^{\,2}}{2} + E_2^{\,2}Cos(2w_2t+\phi_2)Sinc(w_2t)$$

$$+E_1E_2Cos[(w_1+w_2)t+(\phi_1+\phi_2)]Sinc[\frac{(w_1+w_2)T}{2}]$$

$$+E_1E_2Cos[(w_1-w_2)t+(\phi_1-\phi_2)]Sinc[\frac{(w_1-w_2)T}{2}]\}$$

(2.1-44)

The Sinc-function $Sin(x)$ plots in figure2.1-3. As x values increase, y values will decrease rapidly.
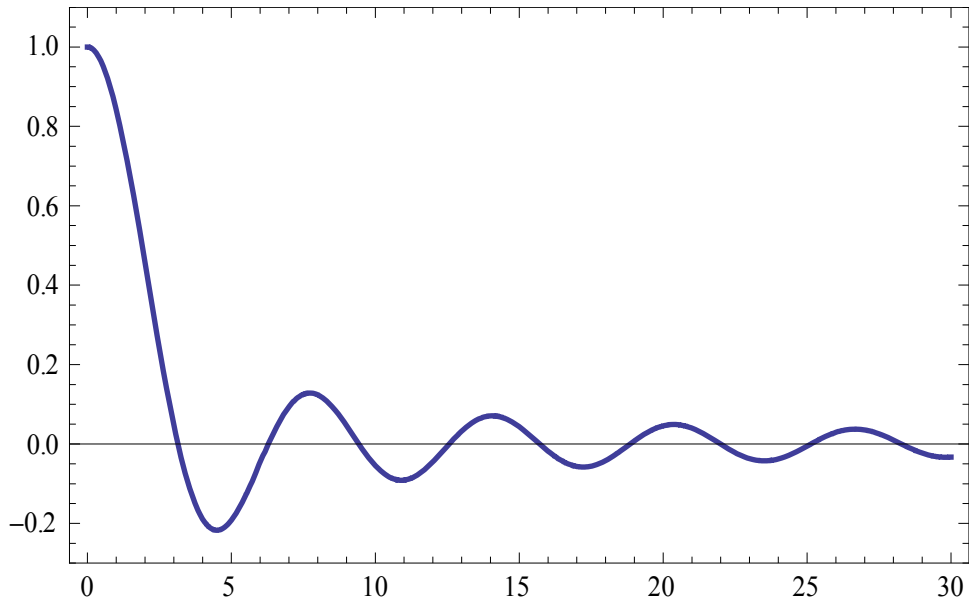
Figure 2.1-3 The plot of Sinc-function

When x values larger then π (3.1415), the y values are small enough to ignore it. The laser frequency is about 10^{15}Hz, but the fast detector response time T is just about 10^{-12}s. We can ignore these faster terms in equation (2.1-26), so the equation can be written as:

$$I_{beat}(t) = \frac{c\varepsilon_0 E_1^{\,2}}{2} + \frac{c\varepsilon_0 E_2^{\,2}}{2} + c\varepsilon_0 E_1 E_2 Cos[(w_1 - w_2)t + (\phi_1 - \phi_2)]Sinc[\frac{(w_1 - w_2)T}{2}]$$
$$= I_1 + I_2 + 2\sqrt{I_1 I_2}\,Cos[\Omega t + \phi]$$

(2.1-45)

The first two terms are the average intensities of wave 1 and wave 2, respectively. Ω is the difference of angular frequency between two waves. ϕ is the phase different of the two waves (figure2.1-4).
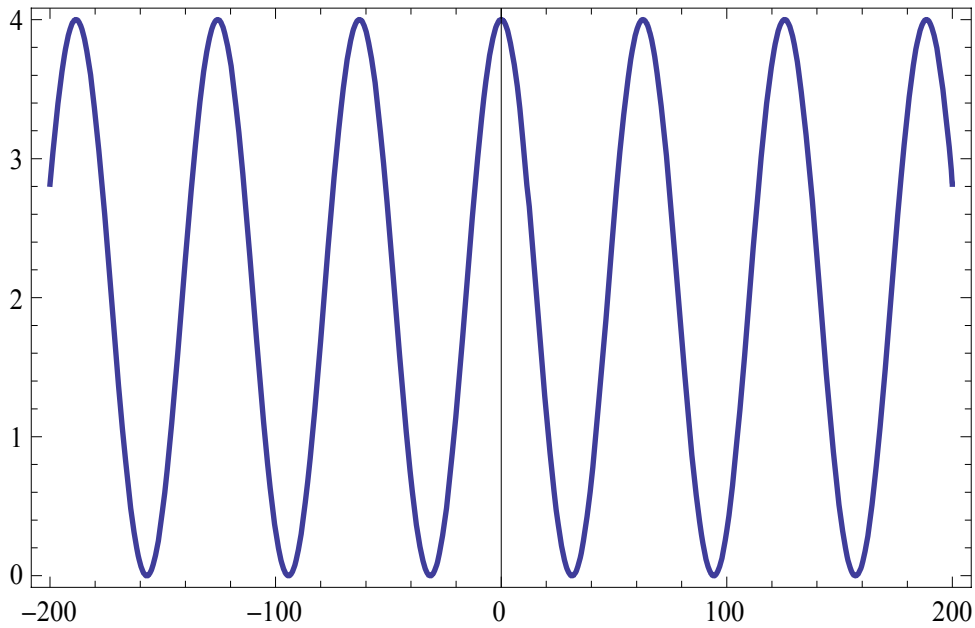
Figure 2.1-4 The beating intensity with an angular frequency of Ω .

In the simulation, we set I_1 equals I_2

2.2 The properties of the material

2.2-1 Choosing and analysis the material

In order to generate high power THz radiation, two properties are necessary for the material. One of properties is long carrier lifetime, and the other is high carrier mobility. Because of them, PC antenna could be generated more current flow which will also increase THz radiation power. Therefore, we can give consideration to two conditions. When we create the more recombination centers in semiconductor, it can trap carriers by using recombination centers to decrease the carrier lifetime. To create the more recombination centers, we implant the more defect in substrate and from deep level recombination. However, implanting

the more defect, the structure of the crystal will be destroyed and decrease the carrier mobility.

$$\tau_c = \frac{1}{N_t \sigma_c <\nu_{th}>} \qquad\qquad (2.2\text{-}1)$$

$$\mu \approx \frac{1.4 \times 10^{22}}{N_t} \frac{m_0 \varepsilon_0}{m^* \varepsilon} \qquad\qquad (2.2\text{-}2)$$

m_0 : the original mass of carrier

m^* : the effective mass of carrier

ε_0 : quasi-static dielectric constant

ε_r : relative dielectric constant

$\varepsilon = \varepsilon_0 \varepsilon_r$

N_t : defect density

μ : carrier mobility

τ_c : carrier lifetime

σ_c : capture cross section

$<\nu_{th}>$: mean thermal velocity

According to the Equation (2.1-1) and (2.1-2), we can know that the longer carrier lifetime the more carrier mobility. It means that we decreasing the carrier lifetime by implanting defects and the carrier mobility also decrease at the same time. Because of it, we use the way which is thermal annealing process to improve it. The thermal annealing processes can rearrangement the crystal of material which implanted defects. It can increase some of the carrier mobility. However, the carrier lifetime also increase.

2.2-2 Dark current

In theory, there is no current generated from PC antenna when we applied voltage across antenna, when it does not illuminate laser beam yet. However, we can measure a few current in PC antenna, which we call dark current. In general, the theory of current transport of the metal-semiconductor junction potential barrier is mainly drift, diffusion, and tunneling effect. It's contribution is in relation to intrinsic potential barrier $q\Phi_B$, built-in electric potential V_{bi} and applied voltage. In order to avoid generating rectification effect and junction resistance on the metal-semiconductor junction, it is usually using the process of implant high concentration of defect in semiconductor to increase built-in electric potential and decrease the width of depletion region. So the carrier can easily through the junction potential as applying voltage. It is the process of Ohm contact.
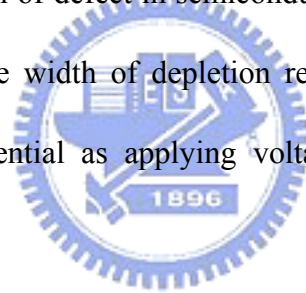
2.2-3 Photocurrent

Comparing with dark current, photocurrent means that CW THz is generated from photoconductive antenna which applies voltage, when it illuminates laser beam. We use the two modes laser to incident into the gap on the photoconductor antenna, we define the optical generation rate g_0 as the number of absorbed incident photons per second, i.e photon flux ($\frac{P_0}{hv}$) per unit volume, multiplied by the optical quantum efficiency η_{opt}, which accounts for reflections at the air-semiconductor interface, as well as for the finite thickness of the

photoconductive layer. Accordingly, we define the optical quantum efficiency as

$\eta_{opt} = \mathrm{T}(1-e^{-\alpha t_{LT}})$, where T is the transmission coefficient at the

air-semiconductor interface and t_{LT} is the thickness of the sample layer. Hence,

the generation rate becomes:

$$g_0 = \eta_{opt}\frac{P_o}{h\nu}\frac{1}{V} \qquad\qquad\qquad (2.2\text{-}3)$$

Where V is the elementary volume associated with the elementary photocurrent

I_{ph} .If we consider n and p the densities of free photogenerated electrons and holes

(assumed spatially homogeneous), we can write the current continuity equation:

$$\frac{dn}{dt} = g_0 - R = g_0 - \frac{n}{\tau_e} \qquad\qquad\qquad (2.2\text{-}4)$$

where $R = \dfrac{n}{\tau_e}$ is the electron recombination rate. In fact, in case of LT-GaAs and

GaAs:O photoconductor one should replace the recombination rate with the

trapping rate. The same equation holds for holes. For an uniformly illuminated

photoconductor, the electron and hole current densities are given only by the drift

components, since there is no diffusion due to the lack of spatial dependence (∂ /

∂ x $\equiv$ 0):

$$J_n = env_e(E)$$
$$J_p = env_p(E) \qquad\qquad\qquad (2.2\text{-}5)$$

where v, e, h is the field-dependent electron (hole) drift velocity. The total current

density is $J = J_n + J_p$, where, at this point the holes contribution to the

photocurrent is discarded due to their low mobility in material. Moreover, the low

mobility of holes produces a small displacement of the hole population in the

external applied field, whereas due to their much higher mobility a significant

number of electrons are displaced into the cathode (+); hence, for maintaining the space-charge neutrality in the illuminated gap and current continuity at the electrodes. A replenishment of electrons at the anode is necessary (i.e. electron injection). The DC photocurrent flowing into the external circuit is given by:

$$I_{ph}^{DC} = Aenv_e(E) \qquad (2.2\text{-}6)$$

where A is the total contact area. With g_0 independent of time, that is $\partial/\partial t \equiv 0$ at steady state, from Eq. 2.2-4, the density of photogenerated electrons becomes:

$$n = \frac{\eta_{opt}}{V}(\frac{P_0}{hv})\tau_e \qquad (2.2\text{-}7)$$

and by substituting it into Eq. 2.2-6 we obtain:

$$I_{ph}^{DC} = e\frac{\eta_{opt}}{d}(\frac{P_0}{hv})\tau_e v_e(E) \qquad (2.2\text{-}8)$$

We can regroup the terms in Equation 2.2-8, by denoting the primary photocurrent $I_{ph}^p = e\eta_{opt}(\frac{P_0}{hv})$ and introducing the photoconductive gain $g = \frac{\tau_e}{t_{tr}(E)}$ where $t_{tr}(E) = \frac{d}{v_e(E)}$ is the photocarrier transit time. In other words, the photoconductive gain is determined by how fast the electrons can transit across the electrodes and contribute to the photocurrent in the circuit before they recombine with the holes, or as in the case of material, they become trapped. In most of the existing designs of photomixers, the carrier transit time is neglected since the transittime for an electrode spacing of ~1 μm is much larger than the carrier lifetime. Forexample, assuming a trapping time of ~1 ps and a drift velocity of ~4.4×10^{6}cm/s,this yields a transit time of ~25 ps and a gain of about 0.04 (<<1), hence the low quantum efficiency of photoswitches. This large

difference between the carrier transit and lifetime means that the photomixer is a carrier lifetime dominated device.

In Eq. 2.2-8, the electron drift velocity is affected by the saturation effects and has the general form:

$$v_e(E) = \frac{\mu_e E}{1 + \dfrac{\mu_e E}{v_{sat}}} \qquad (2.2-9)$$

where μ_e is the carrier mobility and v_{sat} the saturation velocity. At low electric fields one can assume a field-independent mobility, such that $v_e(E) \simeq \mu_e E \simeq \mu_e \dfrac{V}{d}$

Replacing in Eq. 2.2-8, we obtain:

$$I = e \frac{\eta_{opt}}{d} (\frac{P_0}{hv}) \tau_e v_e(E) \qquad (2.2-10)$$

If we now consider the photocurrent modulated at a THz frequency, we can write:

$$I_{ph}^{THz} = \frac{I_{ph}^{DC}}{\sqrt{1 + (w\tau_e)^2}} = e \frac{\eta_{opt}}{d} (\frac{P_0}{hv}) \frac{v_e(E)\tau_e}{\sqrt{1 + (w\tau_e)^2}} \qquad (2.2-11)$$

We can also use the ultra-pulse laser to incident into the gap on the photoconductor antenna, and generate the transient photocurrent to radiate THz electromagnetic pulse. The value of photocurrent is in relation to the bias value and the power of the laser beam. It can express as:

$$I = \frac{V_{bias}}{R_0 + R(t)} = \frac{V_{gap}}{R(t)} \approx \frac{V_{bias}}{R(t)} \qquad (2.2-12)$$

R_0 is time-independence value of resistance. It can divide into two parts, one is contact resistance and the other is load resistance. $R(t)$ is time-dependence value of resistance which photoconductor illuminates laser beam. We set that there is an

incident beam on the photoconductor and using the photon energy generate the electron-hole pair. And then, the photoconductor parameter σ can be expressed as:

$$\sigma=q(\mu_n+\mu_p)\Delta n \tag{2.2-13}$$

where q is the charge of electron, μ_n and μ_p are the mobility of electron and hole. Δn is the density of carrier. If the average power of incident optical pulse is P_{avg} and photon energy is $h\nu$. The carrier generation rate G per unit volume can express as:

$$G=\eta\frac{P_{avg}}{h\nu\tau_{pw}QV_0} \tag{2.2-14}$$

where η is the quantum effect, τ_{pw} is the bandwidth of laser pulse, Q is the repetition rate of laser pulse and V_0 is the total volume of activity region.

Under the steady state, the carrier generation rate G is:

$$G=\frac{\Delta n}{\tau_{pw}} \tag{2.2-15}$$

$$\therefore \sigma=q(\mu_n+\mu_p)\Delta n=q(\mu_n+\mu_p)G\tau_{pw} \tag{2.2-16}$$

From Equation (2.2-16), we can get the optical resistance R_p.

$$R_p=\frac{L}{\sigma A}=\frac{h\nu QL^2}{q\eta(\mu_n+\mu_p)P_{avg}} \tag{2.2-17}$$

where A is the cross-section area of activity region and L is the length of activity region.

From Equation (2.2-12) and Equation (2.2-17), we can express the photocurrent as:

$$I=\frac{V_{bias}}{R_p}=\frac{q\eta(\mu_n+\mu_p)V_{bias}P_{avg}}{h\nu QL^2} \tag{2.2-18}$$

Chapter 3   Experiment Method and Setup

In this chapter, we introduce the samples which are fabricated for our PC antenna. And then, we introduce the experiment methods and setups to measure the emission properties of the THz radiation.

3.1   Sample preparation

We used the dipole antenna as the antenna structure in our experiment. Large signal and high bandwidth can be obtained from this kind of structure [38]. The photoconductive antenna structure is shown in Figure 3.1-1. Knon et al. proved that the spectral response of the PC antenna for broadband detection is mainly determined by the temporal behavior of the number of photo-excited carriers [22].
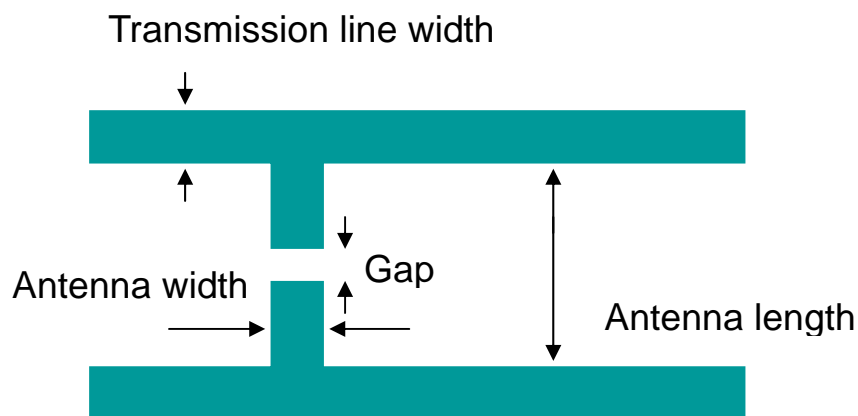

Figure 3.1-1 Schematic diagram of the PC antenna

Recently, Salem et al. [32] improved the characteristics of GaAs substrate and generated THz waves by implanting oxygen ion. Normally, oxygen ion is considered as dust (a disadvantage) for electrical devices fabrication during the process, as its existence will make the contacts to be not Ohmic-contact. But, in the THz generation, it can become advantages. As the electrical level formed by oxygen ion in GaAs is close the Femi-level, it makes the oxygen ion implanted GaAs close to electrically neutral and has comparative high resistance. This kind of material also have high breakdown voltage; and short carrier lifetime by implanted under certain high dosage and annealed under suitable annealing temperature.

3.1-1 Preparation of the PC antenna
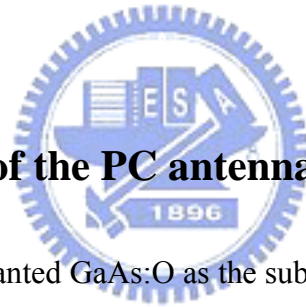
By using multi-implanted GaAs:O as the substrate and then fabricated dipole antenna on it. And our sample is fabricated by KeJian Chen who studies in CUHK. From some groups [29-30, 32], the GaAs:O is further studied. They demonstrated that this kind of material really has some advantages for THz waves generation, and can generate higher power and higher frequency if we can optimize the implant dosage, annealing temperature and introduce some antenna design for high frequency purpose.

By optimize the dosage and the implanted energy to match the requirements. Considering the cost of time for RBS facility, we prepared two kinds of materials which have different carrier life times and mobilities as the same dipole antenna

structure. In implanting process, multi-implants dosage concentrations is 2.5×10^{13} ions/cm^2 (500Kev & 800Kev) and 4×10^{13} ions/cm^2 (1200kev). After implantation process, we performed the thermal annealing by RTA (Rapid Thermal Annealing) under N$_2$ gas environment and use a GaAs cap to prevent As ion absorption. In our experiment, we performed annealing at 500℃ for 60s. (For reference, under 500℃ for 60s annealing, the resistance of this GaAs:O substrate is close to $1.26 \times 10^7 (\Omega/sq)$) and we also measured the carrier life time of both materials by optical-pump probe measurement. The carrier life time of GaAs:O is 550fs and LT-GaAs is 700fs. The fitting curve are shown in figure 3.1-2
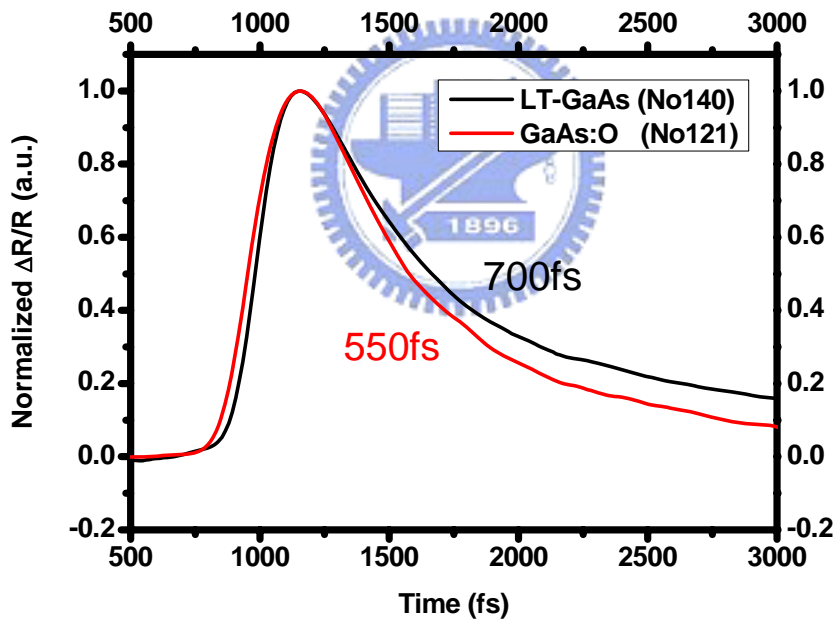

Figure 3.1-2 The measurement of carrier life time with both materials

We also calculated the conductivity of GaAs:O and LT-GaAs. The conductivity of GaAs:O is 3.8x10$^{-2}\Omega^{-1}$cm^{-1} and LT-GaAs is 1.7x10$^{-4}\Omega^{-1}$cm^{-1}, the measurement are shown in figure 3.1-3.
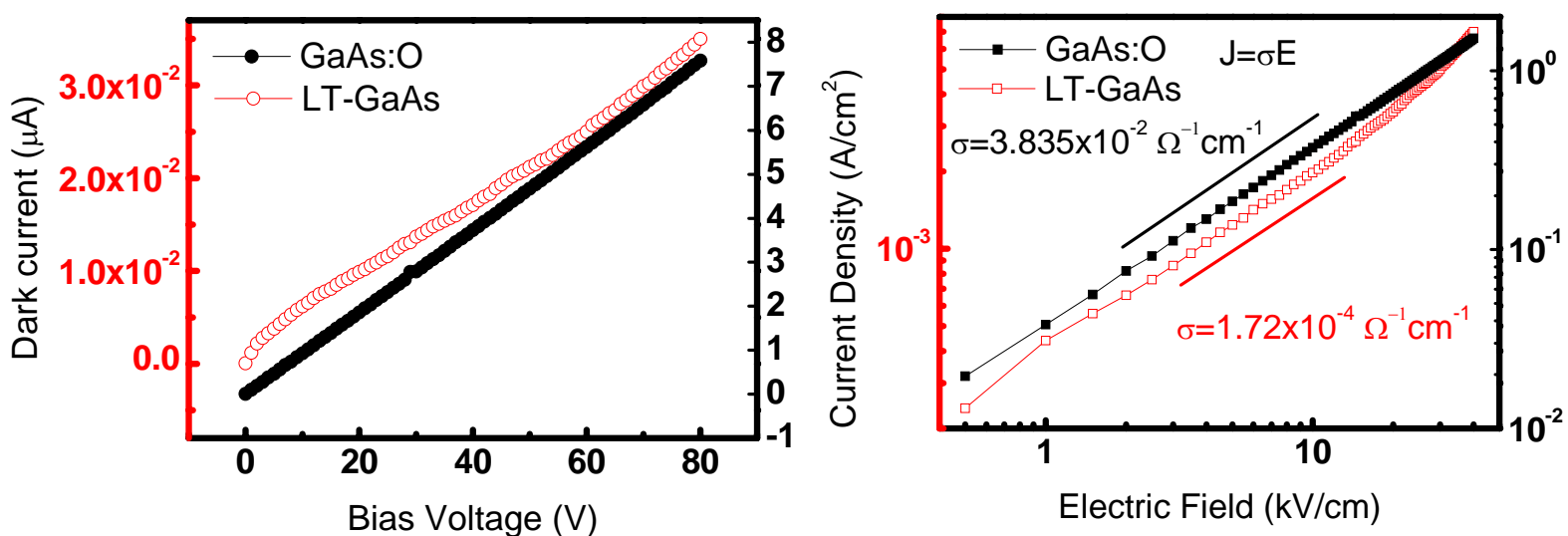
Figure 3.1-3 The measurement of dark current and conductivity of GaAs:O and

LT-GaAs

3.1-2　The setup of PC antenna

After preparing the PC antenna, we put the PC antenna on the mount which we designed. We used objective lens to focus pump laser on the dipole antenna. And then, we used the silicon lens to decrease the angle of the THz radiation outgoing the substrate. The type of our silicon lens is hyper-hemispherical lens, the radius is 6.75mm and the total thickness is 8.35mm. In order to make sure the right position of laser beam, we used two steps. For the first step, we used a thin glass and put it before the objective lens. Then, we can see the image on the screen reflected from the dipole antenna and check the location of focused laser beam on the sample. The detail experiment method is shown in the Figure 3.1-4. After checking the correct location the next step was to contact the multi-meter to the dipole antenna for measuring the resistance, and then optimized the objective lens

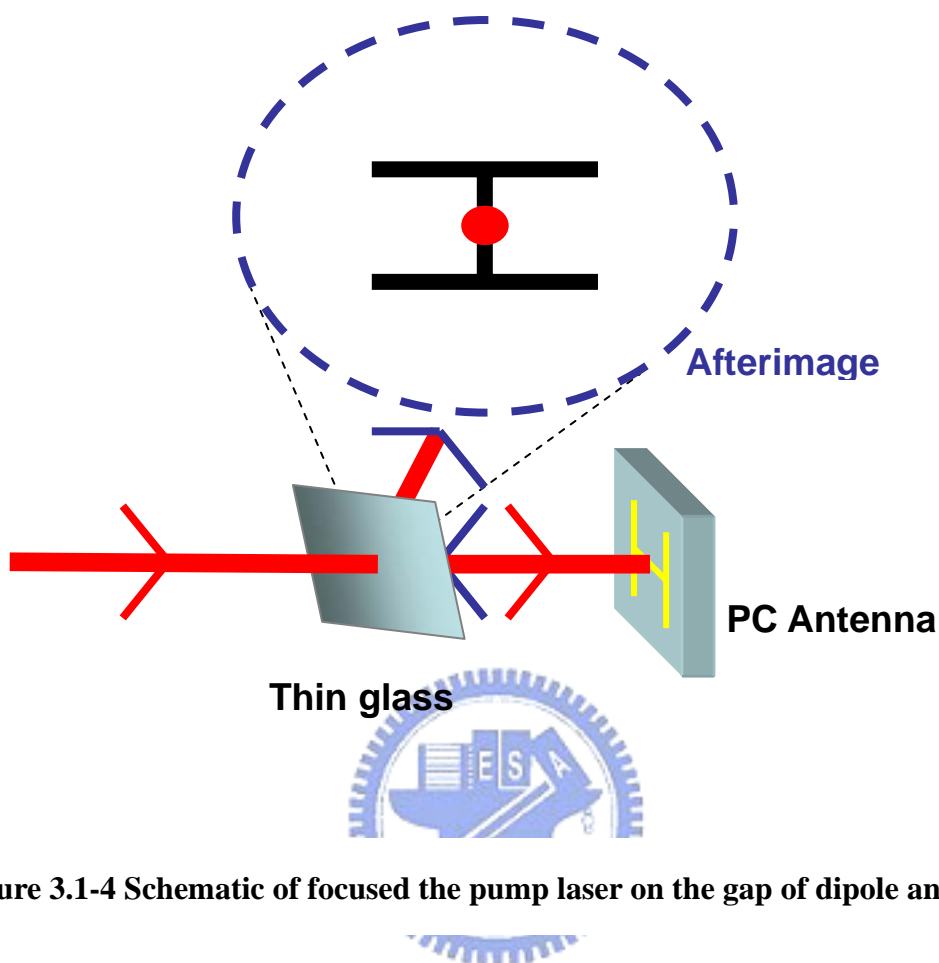and incident pump beam until search the minimum value of resistance was found.

Figure 3.1-4 Schematic of focused the pump laser on the gap of dipole antennas.

3.2 Dual wavelength laser diode system

3.2-1 Laser diode characteristics

In order to measuring the better THz radiation power, we directly excited our PC antenna by using two frequency-independent circular laser diodes (SANYO DL-8032-001) with output power 57mW and wavelength around 830nm. The L-I curve of the laser diodes are showing in Fig. 3.2-1 and Fig 3.2-2
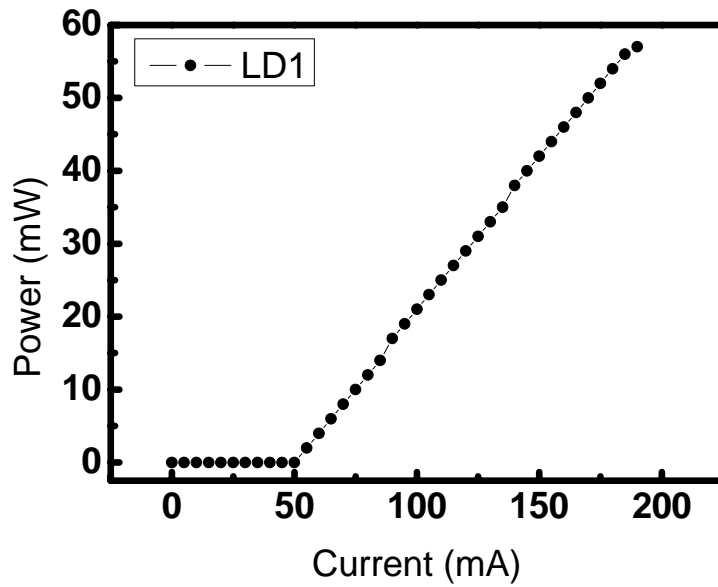
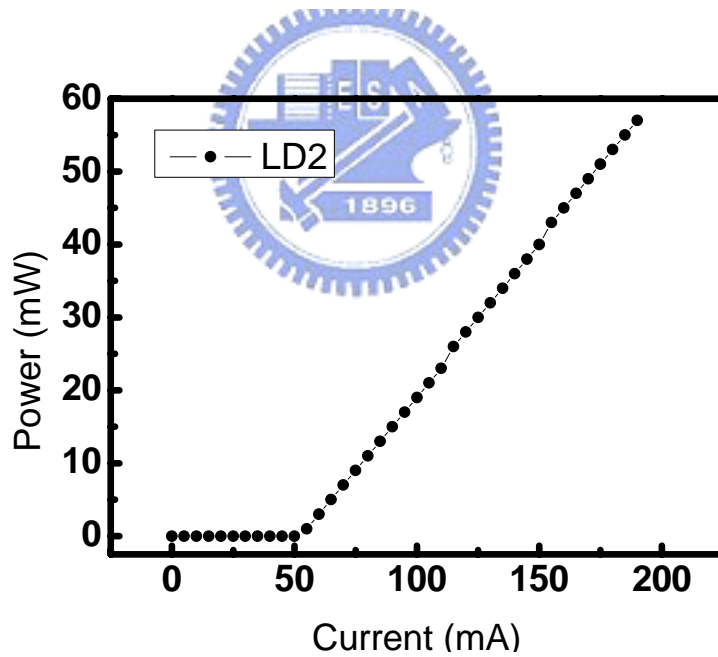**Figure 3.2-1 L-I curve of laser diode 1 (LD1), I$_{th}$=50mA**

Figure 3.2-2 L-I curve of laser diode 2 (LD2), I$_{th}$=50mA

The linewidth of LD1 and LD2 measured by Fabry-Perot interferometer are

shown in Fig 3.2-3 and Fig 3.2-4, where their linewidth are 22MHz and 21MHz,
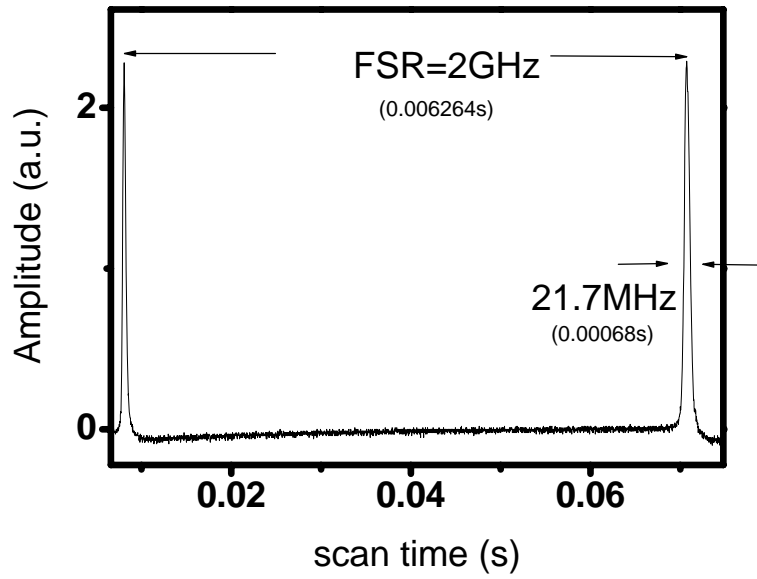
respectively.

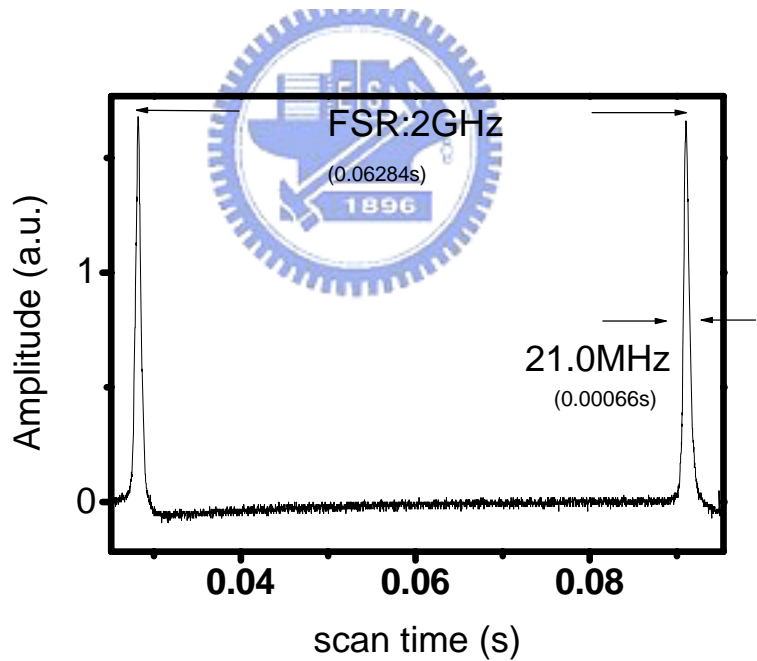**Figure 3.2-3 Linewidth of LD1 measured by Fabry-Perot**

Figure 3.2-4 Linewidth of LD2 measured by Fabry-Perot

In our experiment, we can get CW the THz radiation with different central frequency by tuning the wavelength of each LD. Therefore, by controlling the operation current and temperature, we can tune the wavelength difference between

the two laser diodes. The accuracy of the current driver (New port 505B) and the temperature controller (New port 325B) are ± 0.004mA and ± 0.1 ℃ respectively.
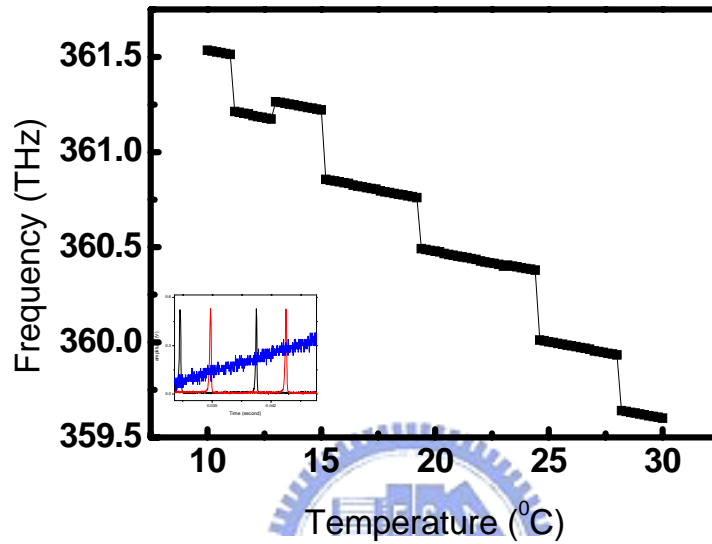

Figure 3.2-5 Temperature control at current 190mA for LD1.

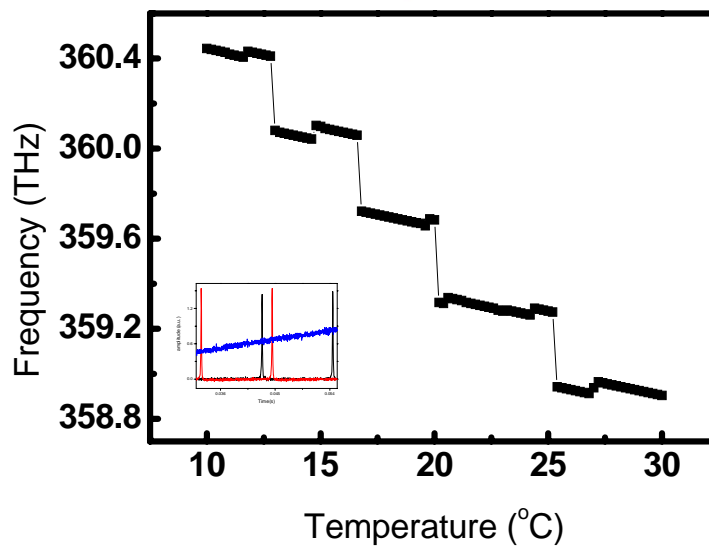**The inset picture is Fabry-Perot interferogram of the laser diode 1.**

Figure 3.2-6 Temperature control at current 190mA for LD2.

The inset picture is Fabry-Perot interferogram of the two laser diodes.
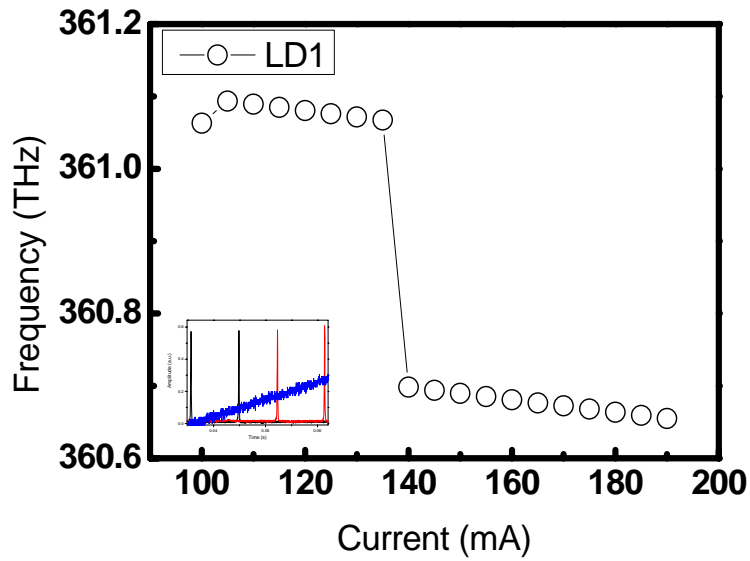
Figure 3.2-7 Current control at 23℃ for LD1.

The inset picture is Fabry-Perot interferogram of the laser1.
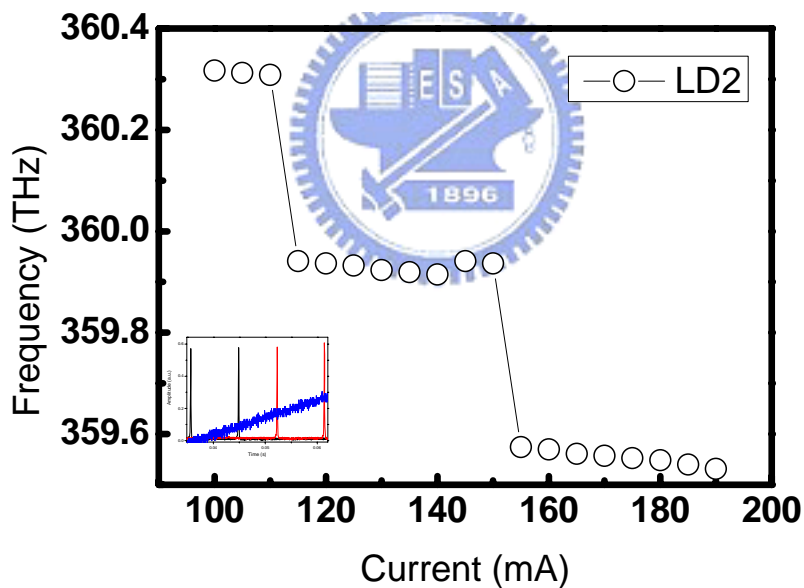
Figure 3.2-8 Current control at 23℃ for LD2.

The inset picture is Fabry-Perot interferogram of the laser2.

In figures 3.2-5 and fig 3.2-6, the wavelength shift caused by changing temperature are 11.6GHz/℃(LD1) and 13.2GHz/℃(LD2) ; the shift caused by shifting current are 2.3GHz/mA(LD1) and 2.1GHz/mA(LD2).

We used Fabry-Perot interferometer to measure the frequency stability of the two laser diodes. We recorded the fluctuation of frequency of two laser diodes on the oscilloscope around 20 minutes. The individual frequency shifts of LD1 and LD2 are 416 MHz and 554.MHz, respectively.
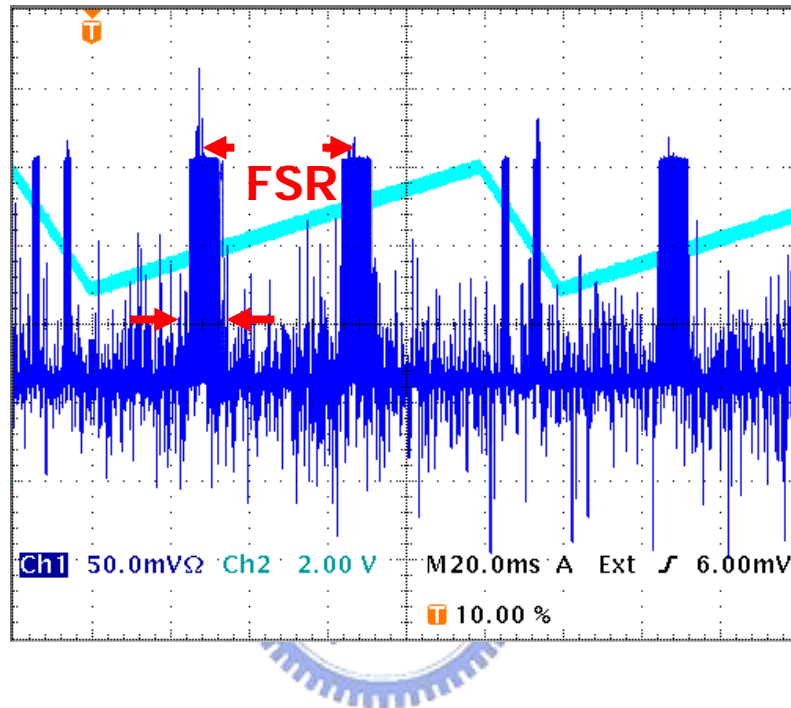
Figure 3.2-9 Frequency fluctuation of LD1 in 20 minutes
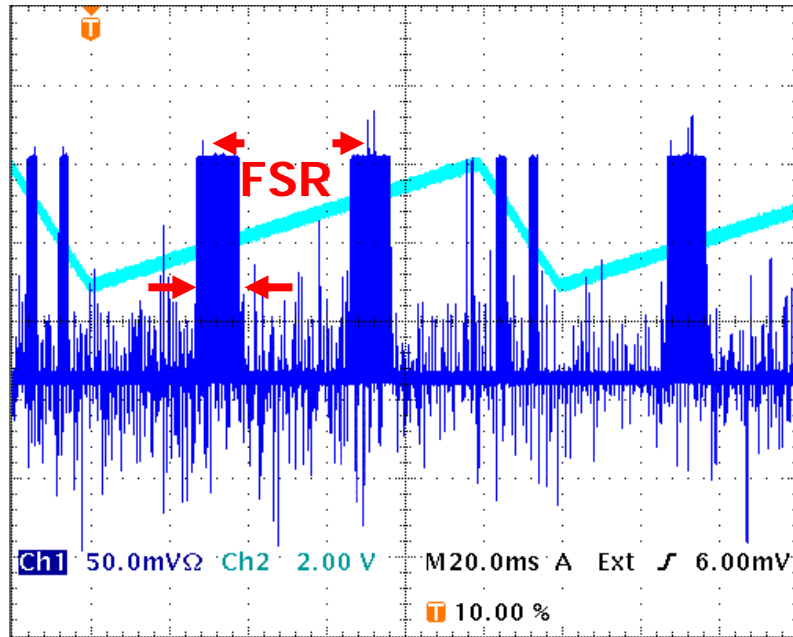
Figure 3.2-10 Frequency fluctuation of LD2 in 20 minutes

Table 3-1 is a brief summary of the characteristics of the two laser diodes

	LD1	LD2
wavelength	~830nm	~830nm
Power	57mW@190mA	57mW@190mA
linewidth	22 MHz	21 MHz
Current v.s. frequency	2.3GHz/mA	2.1GHz/mA
Temperature v.s. freqency	11.6GHz/℃	13.2GHz/℃
Frequency fluctuation	416MHz@20mins	554MHz@20mins

Table 3.1 A brief summary of the characteristics of the two laser diodes

3.2-2 Dual-wavelength laser diodes system

Our dual-wavelength light source system is presented in figure 3.2-7. It is composed of two frequency-independent laser diodes and some proper optics. The polarization of the LD is S polarization. The 40X objective lens are used to focus the spot size of the two LD, when light passes through the isolator, the polarization of the incident light will rotated to 45^0 to prevent the optical feedback from other optics, when the light passes through the half-wave plate, the polarization will be changed from linear polarization to elliptical polarization.
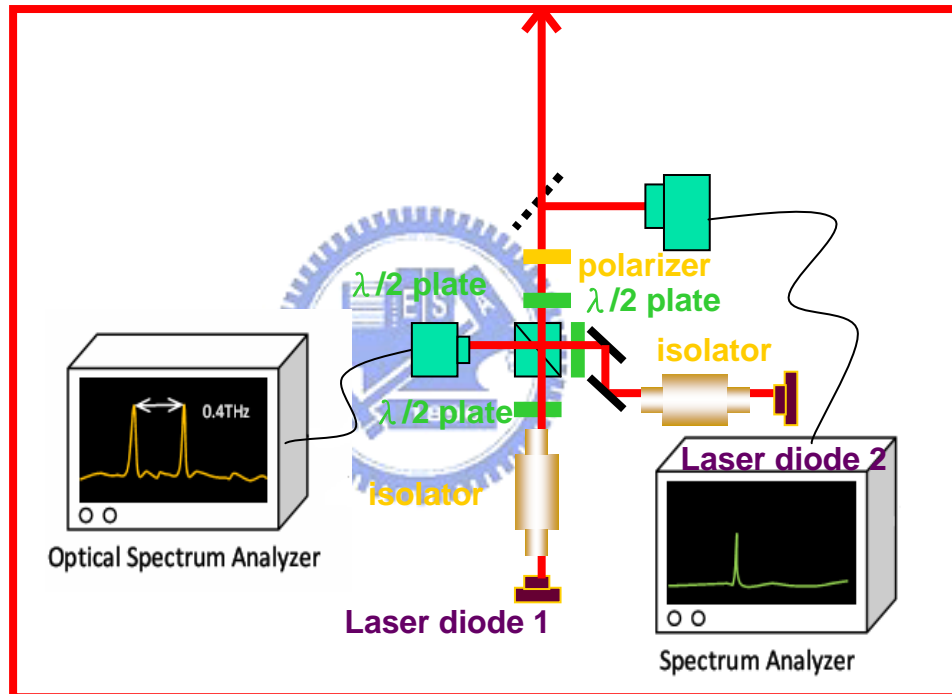
Figure 3.2-9 schematic of dual-wavelength system

We measure the output spectrum by optical spectrum analyzer (OSA, MS 9030, resolution 0.01nm) is shown in figure 3.2-8.
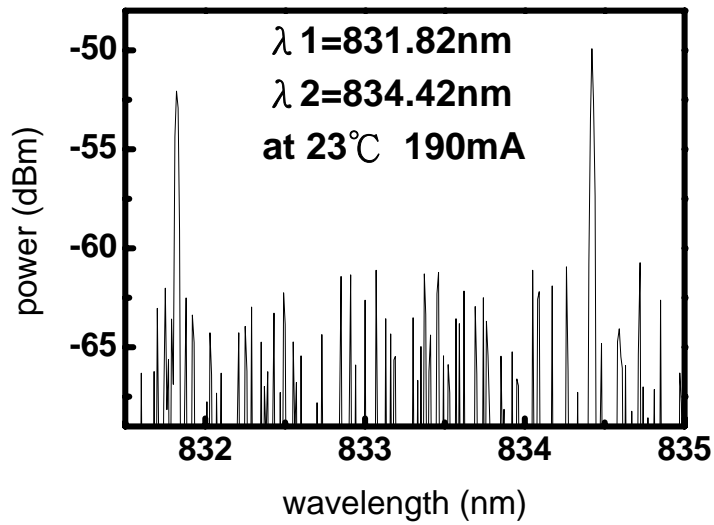
Figure 3.2-10 The spectrum of 2 laser diodes system

To optimize beating efficiency, we need RF spectrum to check it. Because the maximum frequency can be detected from our spectrum analyzer is 3GHz, we must adjust the frequency difference of two laser diodes lower than 3GHz.The low frequency beating signal is shown in figure 3-.2-8
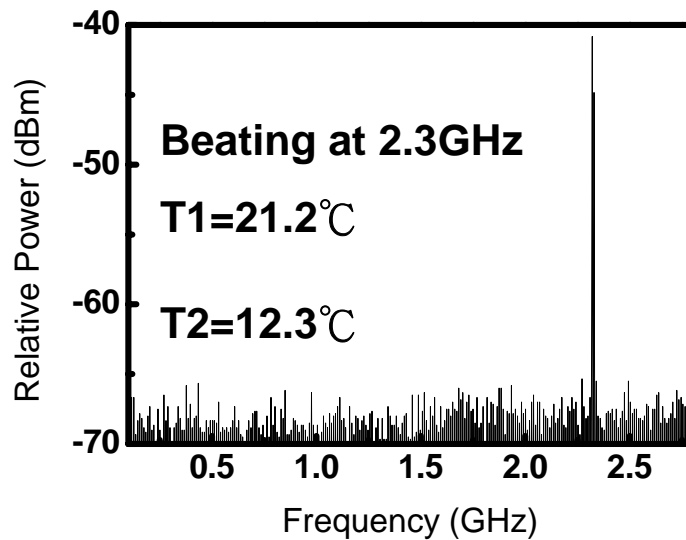
Figure 3.2-11 The beating signal of the PC antenna

3.3   Experimental setup of generation and detection of THz

3.3-1   Experimental setup

The emitted THz radiation was collimated and focused by a pair of off-axis parabolic mirrors onto the detector. We used a High-Voltage Source Meter (Model2410) to provide bias to the PC antenna and measure the current-voltage curve. To measure total THz power, we used a 4.2 K liquid-helium-cooled Si bolometer as our detector, which was carefully calibrated with a blackbody radiation source. The experiment setup for generation and detection of THz radiation is shown in Figure 3.3-1.

Figure 3.3-1 Schematic of experimental setup for measure the electric characteristics of PC antenna

3.3-2　The calibration of the Si bolometer

We need to calibrate our meter first before using bolometer to detect THz radiation. The output of the bolometer is a voltage signal. We used a blackbody radiation as the standard thermal source to the bolometer for calibration. Due to the literatures [40-41], we can get the following equation (3.3-1).
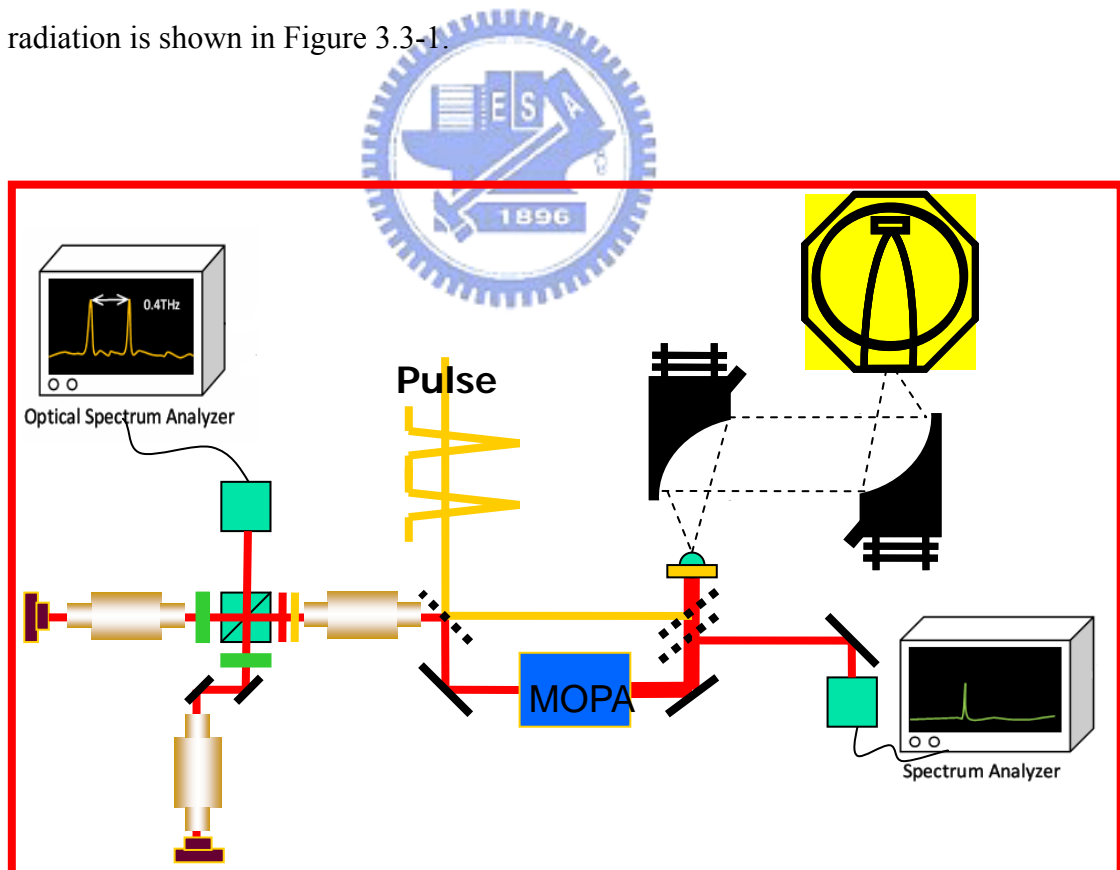
$$R_{peak} = \frac{V_{output}}{\frac{A_{BB}A_d}{R^2} F_F \int_{\lambda_1}^{\lambda_2} R(\lambda) \frac{M(\lambda,T)}{\pi} d\lambda} \tag{3.3-1}$$

Where λ_1 and λ_2 are the cut-on and cut-off wavelength, which we set form $100\,\mu m$ to $3000\,\mu m$, in the response spectrum of our Si bolometer limited by the window filter. R_{peak} is the peak response in the response spectrum. R is the distance between the bolometer and the blackbody radiation source. A_{BB} and A_d are the area of aperture in the blackbody radiation source and the detective window of bolometer, respectively. $R(\lambda)$ is the response spectrum of the bolometer which is assumed to have a rectangle shape due to that the response of the Si bolometer is nearly independent of the frequencies from cut-on to cut-off wavelength, although the response of the Si bolometer actually decrease with the decrease of the frequency slightly. V_{output} is the voltage value which we obtain in lock-in amplifier. F_F is the modulation parameter of chopper, which is about 0.5. The experiment setup is shown in figure 3.3-1. Then, $M(\lambda,T)$ is the absolute power spectrum of the blackbody radiation source, which is the function of wavelengths and temperatures. The formula is given as following equation (3.3-1).

$$M(\lambda,T) = \frac{3.73 \times 10^4}{\lambda^5 (e^{\frac{14388}{\lambda T}} - 1)} \tag{3.3-2}$$

where the unit is $Wcm^{-1}\mu m^{-1}$. There is the experiment setup show after calibrate bolometer, we know that the obtained response is about 5.26 mV per μW with the preamplifier gain set to 200 chopping frequency. So we can use the information of the voltage value we measure in experiment to calculate the energy power of THz radiation.

3.3-3 Semiconductor Laser Amplifier (MOPA)

The output power of single mode laser diodes is very limited and not sufficient for a variety of applications. In order to have higher output power, the output beam of the laser diodes is coupled into an amplifier with a tapered gain region. For this, the collimated beam of the laser diodes is focused on the entrance facet of the amplifier laser diode. The amplifier has an anti-reflection coating on both facets to prevent laser emission without seeding.

Because of the broad gain profile, the so-called" Tapered amplifiers" have a wide tuning range of some ± 20 nm depending on the center wavelength.

We use TOPTICA Photonics AG BoosTA semiconductor Laser Amplifier and also test amplifier gain. Figure 3-2 shows that gain of amplifier with different wavelengths.
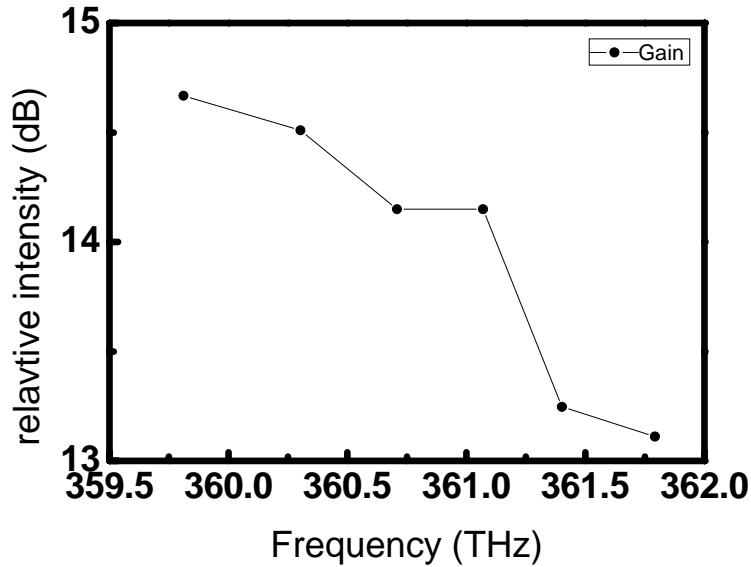
Figure 3.3-2 Frequency dependence of amplifier gain

3.4　The time & frequency domain of THz pulse

In order to measure the time and frequency domain of THz properties generated from PC antenna, we used Time-Domain Spectroscopy system (THz-TDS) which can get time and frequency domain THz radiation information.

3.4-1　Terahertz Time-Domain Spectroscopy (THz-TDS)

Figure 3.4-1 shows that Terahertz Time-Domain Spectroscopy (THz-TDS) experimental setup. The incident pump pulse was focused by an objective lens on the biased gap of the PC antenna to generate THz radiation. The THz radiation was collimated and focused by a pair of off-axis parabolic mirror on a PC sampling detector which was also a PC antenna mounted on the back of a Si hemispherical lens. The PC detector was gated by femto-second probe beam pulses that were separated from the pump beam pulses by a beam splitter, and the DC photocurrent was induced by the incident electric field of THz radiation on the

PC detector. Using delaying the time of the probe pulse to the pump pulse, the time-domain waveform of the electromagnetic pulse was obtained. The time resolution was limited by the carrier lifetime of the LT-GaAs used for the PC detector. To increase the signal-to-noise ratio, the pump beam was modulated with a mechanical chopper at 1 KHz, and output signal from the PC detector was measured with a lock-in amplifier and stored by the computer.
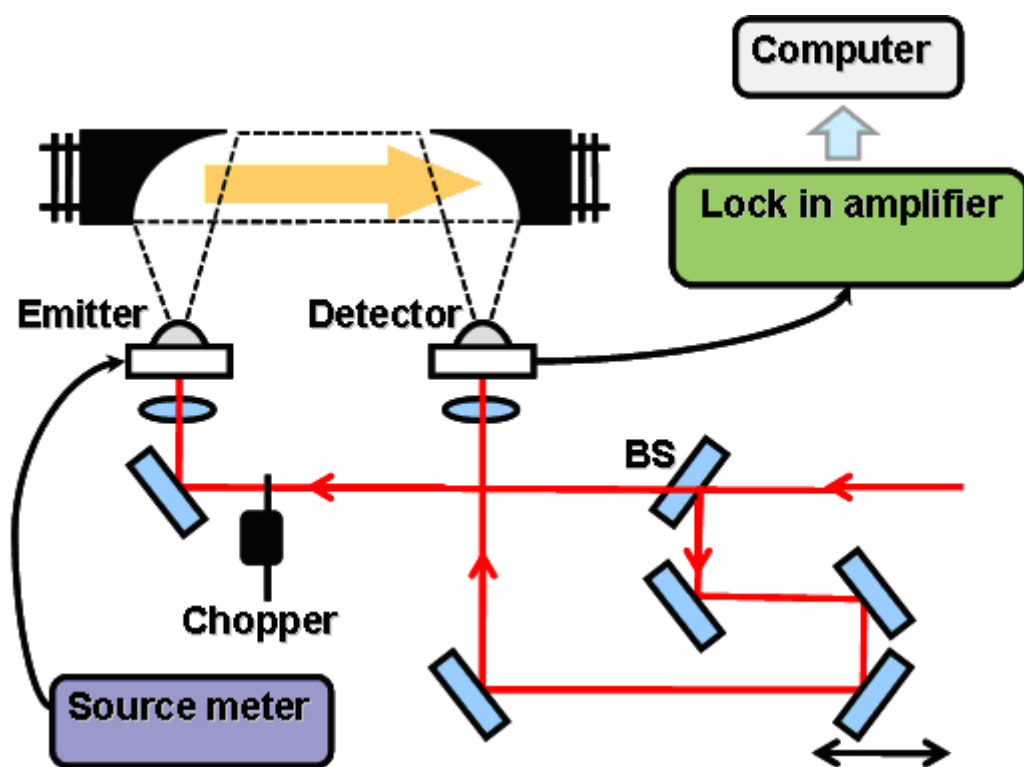
Figure 3.4-1 Terahertz Time-Domain Spectroscopy system

Chapter 4   Result and Analysis

In chapter 4, we demonstrate and analyze the experiment results of THz emission properties of GaAs:O (Oxygen ion implanted GaAs) and LT-GaAs (Low temperature grown GaAs) PC (photoconductive) antenna under pulse laser pumping and continuous-wave laser pumping. We use the same antenna structure fabricated on two different materials. Figure 4.1 show that detail antenna structure.

25μm

25μm

20μm

170μm

Figure 4.1 The structure of PC antenna fabricated on GaAs:O and LT-GaAs material

4.1   The result of pulse measurement

4.1-1   Current-voltage (I-V) curve

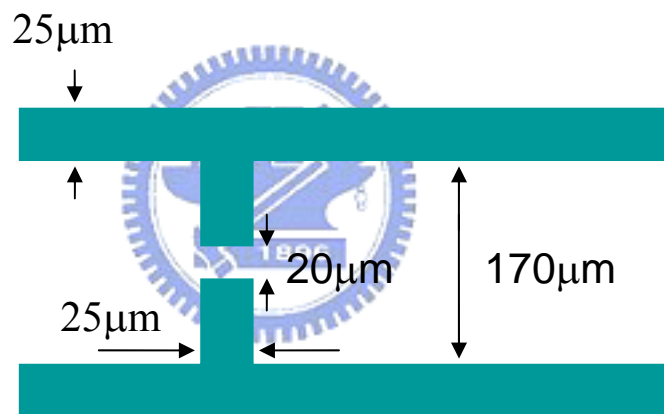Figure 4.1-1 shows the current-voltage characteristics result of the PC dipole antenna with the same structure, one of material is GaAs:O and the other is LT-GaAs. The beam illuminated at the gap of PC antenna, with incident power of 30mW. We also measured the dark current which was without the pump power. It can easily confirm from Figure 4.1-1 that the I-V curve is a linear curve at low bias voltage and a quadratic curve at higher bias voltage. This means that the current is proportion to the bias we gave at low bias voltage and quadratic proportion to higher bias voltage. We can observe that increasing ratio of GaAs:O is higher than LT-GaAs. We observe that the dark current of the GaAs :O is higher than LT-GaAs, the net photocurrent of GaAs:O is 3 times to that of the LT-GaAs when the bias is at 80V and there is no saturation effect in current bias curve for both materials pumping with pulse laser.
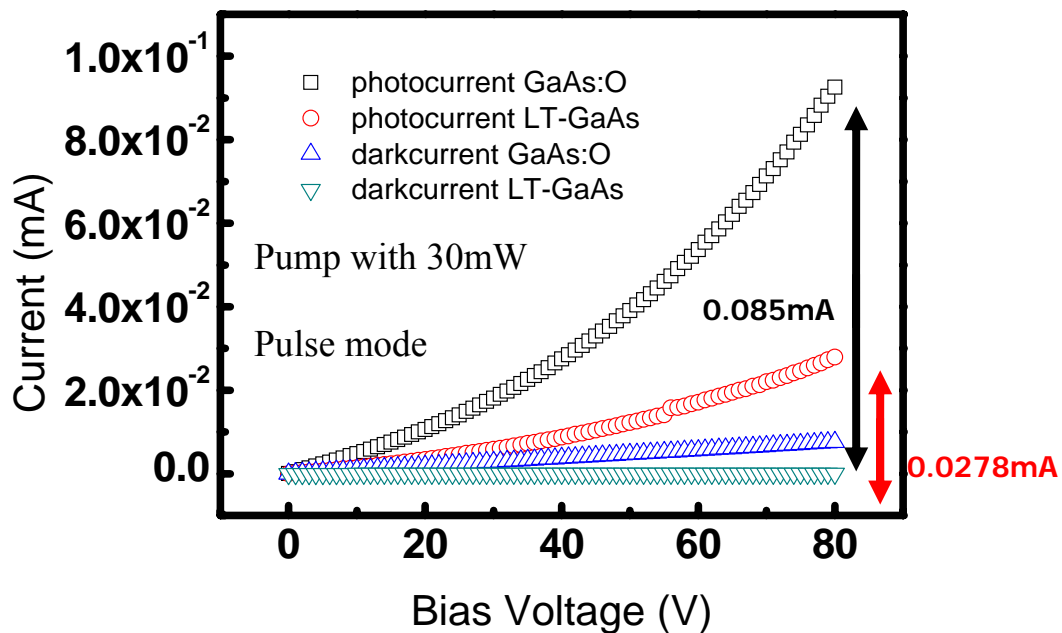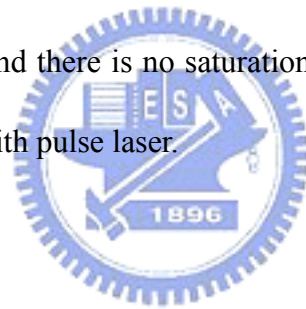
Figure 4.1-1 I-V curve of GaAs:O antennas and LT-GaAs antennas with the same antenna structure source under pulse laser pumping

4.1-2 THz power-voltage curve

Figure 4.1-2 shows the bias voltage dependence of the THz absolute intensity generated from different material with the laser beam focused near its anode with the same antenna structure. They were detected by the bolometer. According the Figure 4.1-2, we can observe that the THz power increases quadratically with the bias at higher bias voltage. GaAs:O has higher photocurrent than LT-GaAs, and GaAs:O has high power when we biased higher than 60V. The THz peak power of GaAs:O is 5.2mW and LT-GaAs is 3.6mW when biasing at 80V and pumping with 30mW. GaAs:O generate pulse THz power almost 1.4 times LT-GaAs. The increasing ratio of THz power-bias voltage curve of GaAs:O are higher than LT-GaAs, although LT-GaAs has higher THz power at lower bias voltage. And there is no saturation effect in both materials under pulse laser pumping.
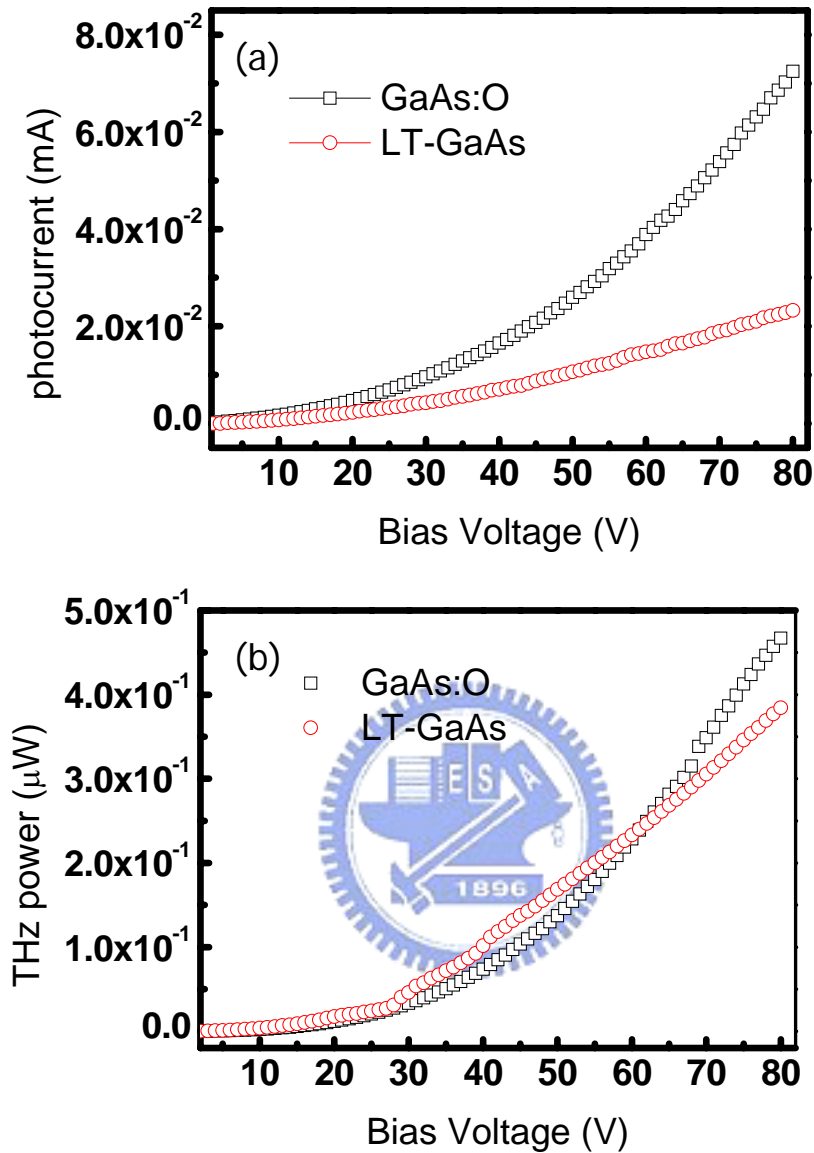
Figure 4.1-2 (a) Photocurrent-bias (b)THz power-bias curve of GaAs:O and

LT-GaAs antenna with the same antenna structure

4.1-3　THz TDS measuerment

We used TDS to characterize the GaAs:O and LT-GaAs antenna. Figure 4.1-3 shows that THz wave form of GaAs:O and LT-GaAs. The measurements are under different bias voltage (20V、40V、60V、80V) and pump power is fixed at 30mW.
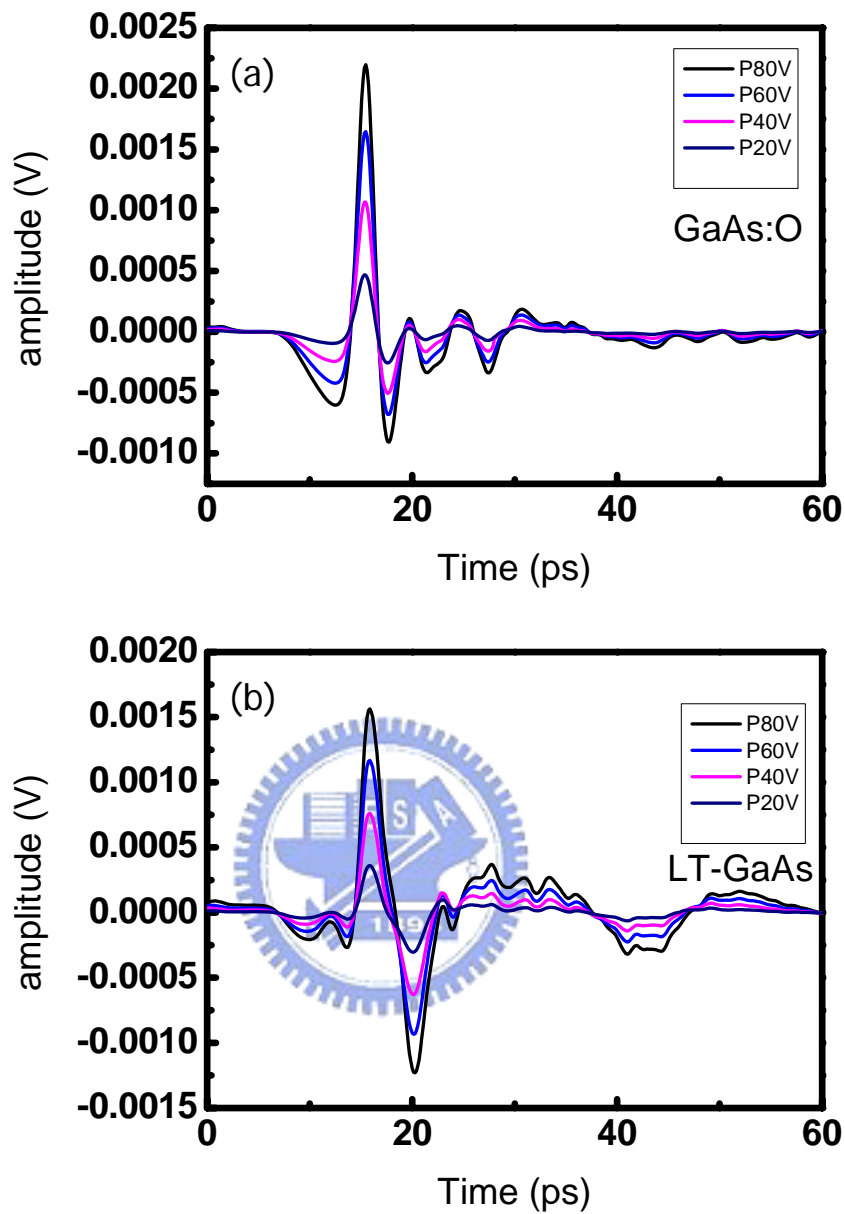
Figure 4.1-3 THz time domain waveform of (a) GaAs:O and (b) LT-GaAs at

constant pump power 30mW

The THz spectra under different biases are shown in figure 4.1-4. We observed that the THz peak amplitude increases when bias increases, However, we can't observe any spectral shift, and this also matches with previous literature[24].

.
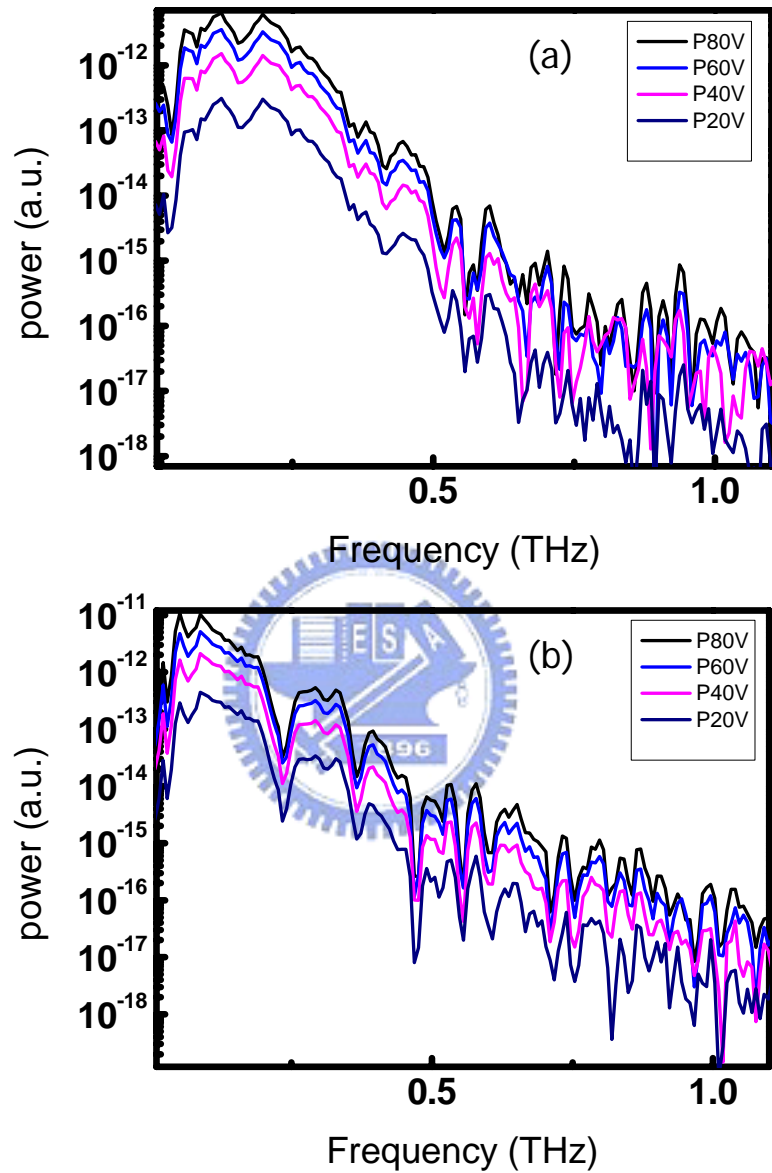
Figure 4.1-4 THz spectrum of (a) GaAs:O and (b) LT-GaAs at constant pump

power 30mW

Figure 4.1-5 (a) show that the main peak amplitude of GaAs:O is higher

than LT-GaAs under pump 30mW and bias 80V in pulse mode. And we observed

both spectra are about 1THz.
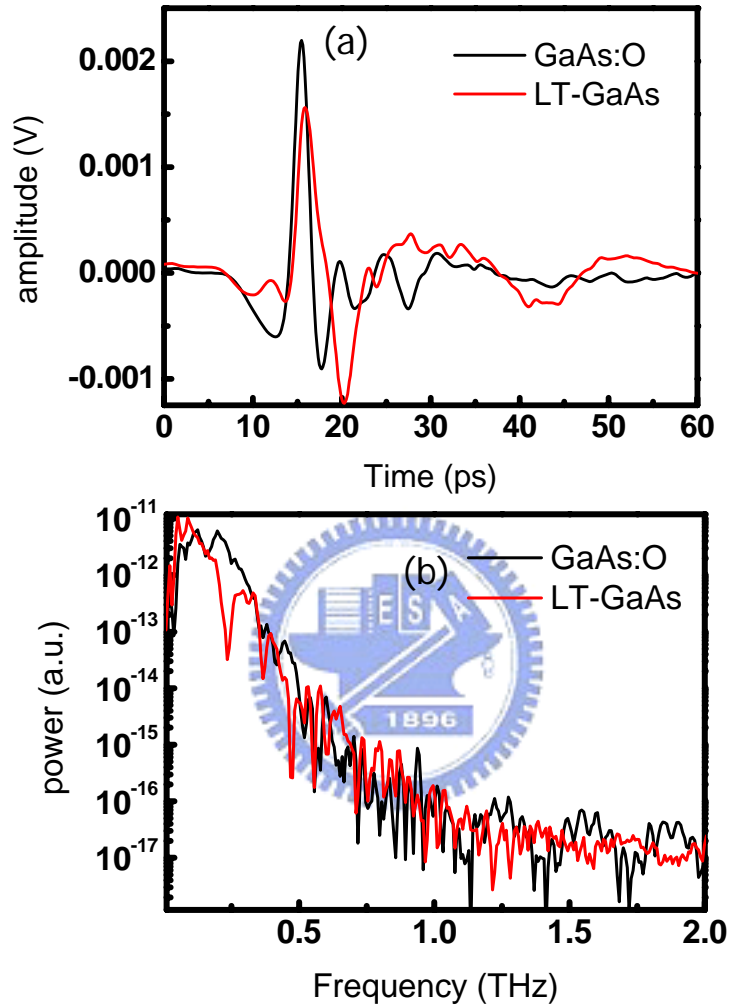
Figure 4.1-5 (a) Time domain waveform (b) Spectrum for both materials

4.1-4   Analysis and Discussion

Figure 4.1-6 (a) shows the pump power dependence of the THz intensity

measured for our PC antennas using a constant bias voltage of 80V. Figure 4.1-6

(b) shows the bias voltage dependence of the THz intensity measured for our PC antennas using a constant pump power of 30mW. Due to the low pump power, we can not observe the strong saturation effect in Figure 4.1-6 (a) in pulse mode. Because the pump power doesn't excite enough carriers to form reverse electric field. And also we can't observe the saturation effect in Figure 4.1-6 (b) due to the low electric field. .
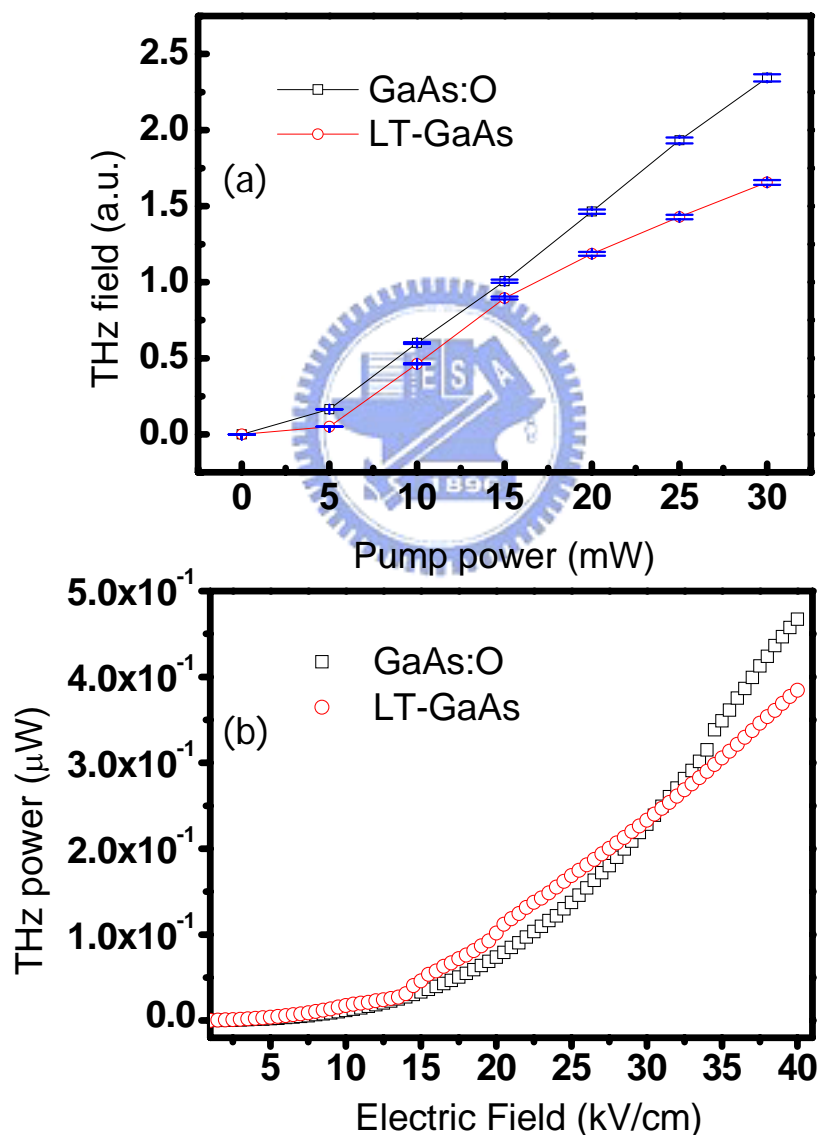
Figure 4.1-6 (a) The amplitude-pump power curve at bias voltage 80V (b) The

THz power-electric field curve at 30mW.

We can see the shift in time domain waveform in both materials. And they are shown in figure 4.1-7, the phenomena of shift of the waveform to earlier time delay is explained by the scattering of photoexcited electrons from the high-mobility Γ valley to the low-mobility L valley, resulting in the wave form shift to the earlier time delay[24]. The intervalley scattering effect is expected to be more significant is LT-GaAs, due to the longer carrier life time.

Figure 4.1-7 (a) GaAs:O (c) LT-GaAs time domain waveform under different bias voltage. The inset figure is relative shift (b) GaAs:O (d) LT-GaAs peak shift- bias voltage curve

4.2 The result of CW measurement

4.2-1 Current-voltage (I-V) curve

In this section we used two frequency dependent laser diodes to produce beating at THz frequency. Then we illuminated laser beams to the antenna with the same structure under different fabricated material. Figure 4.2-1 shows the current-voltage characteristic result, one of material is GaAs:O and the other is LT-GaAs. The incid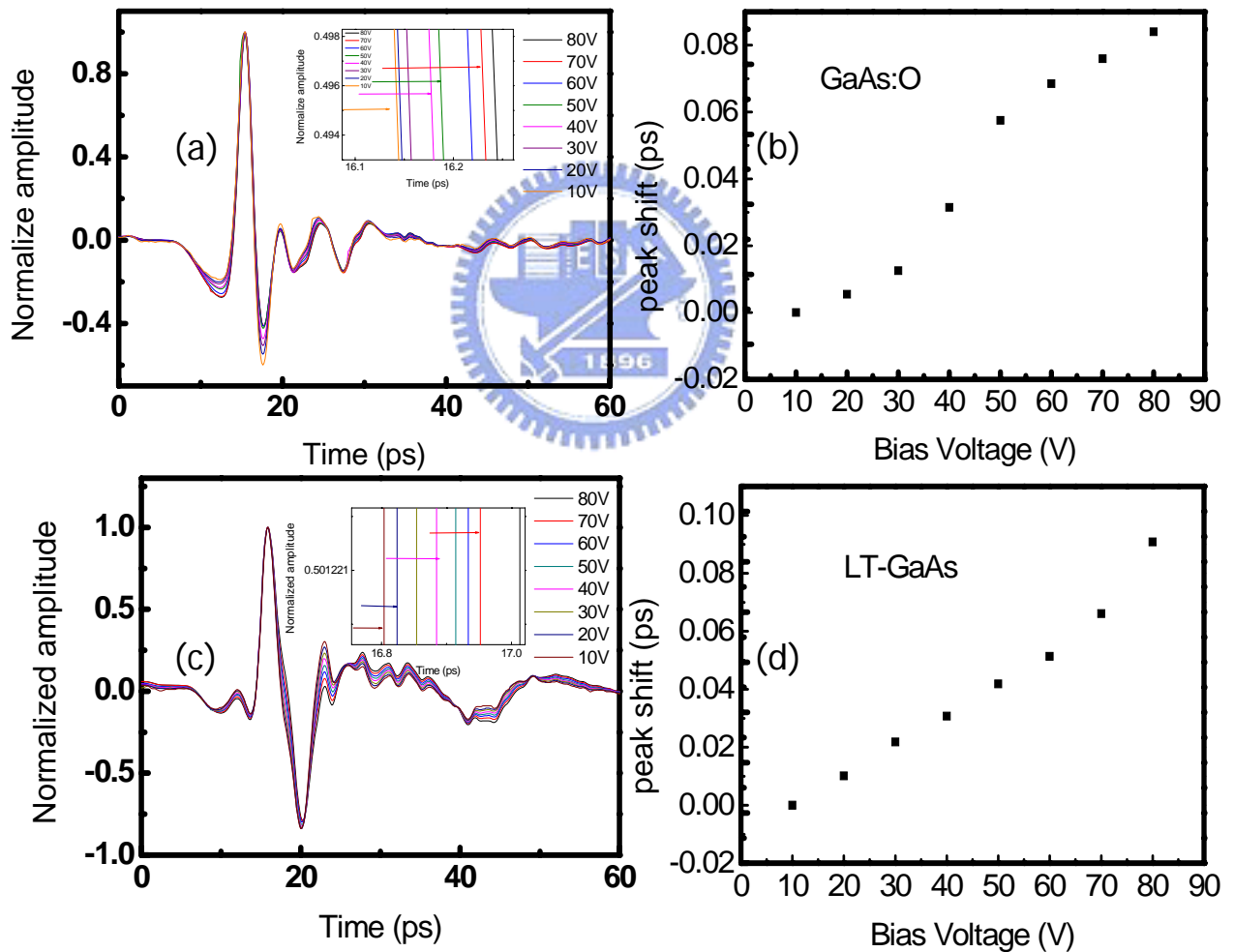ent power was 180mW and the beam illuminated to the gap of PC antenna. We measured the dark current without pump power before. It can easily confirm from Figure 4.2-1 that the I-V curve is a linear curve at high bias voltage and a sub-linear curve at lower bias voltage, the sub-linear region is due to the electron drift velocity saturation [45] and super-linear region is due to the increase of carrier life time [46], and it means that the current is proportion to the bias we gave at higher bias voltage and sub-linear proportion to lower bias voltage. We can also observe that increasing ratio of GaAs:O is higher than LT-GaAs. Although that the dark current of the GaAs:O is higher than   LT-GaAs, the net photocurrent of GaAs:O is 3 times to LT-GaAs and there is no current saturation effect in both material pumping with CW laser.
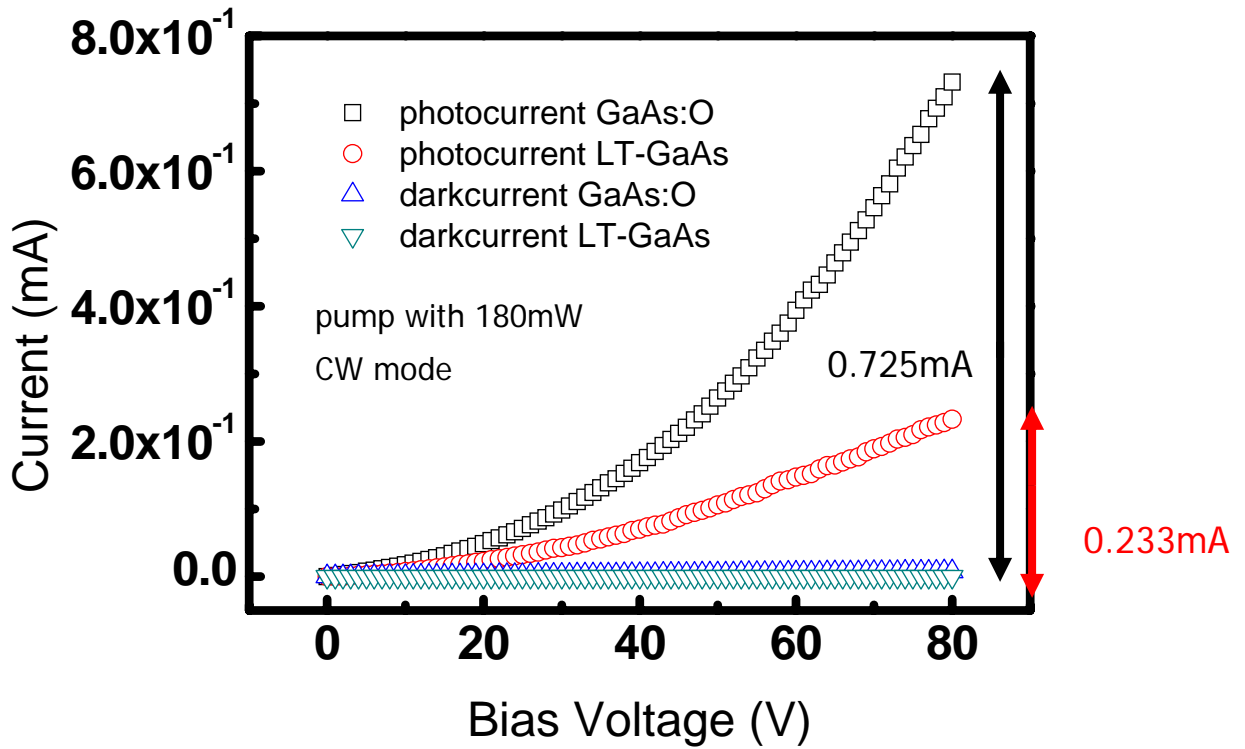
Figure 4.2-1 I-V curve of GaAs:O antennas and LT-GaAs antennas with the same antenna structure source under CW laser pumping

4.2-2 THz power-voltage curve

Figure 4.2-2 shows the bias voltage dependence of the photocurrent and the THz absolute intensity generated from different materials with the two laser beams focused near its anode with the same antenna structure. They are also detected by the bolometer. According the Figure 4.2-2, we can obtain that the THz power are almost the same for both materials when bias is smaller than 40V, the highest THz power of GaAs:O is 2.268μW and LT-GaAs is 1.27μW. GaAs:O has almost 1.8 times to LT-GaAs and there is no saturation effect in high bias voltage. However we observe THz power saturation effect in low temperature grown GaAs [48].
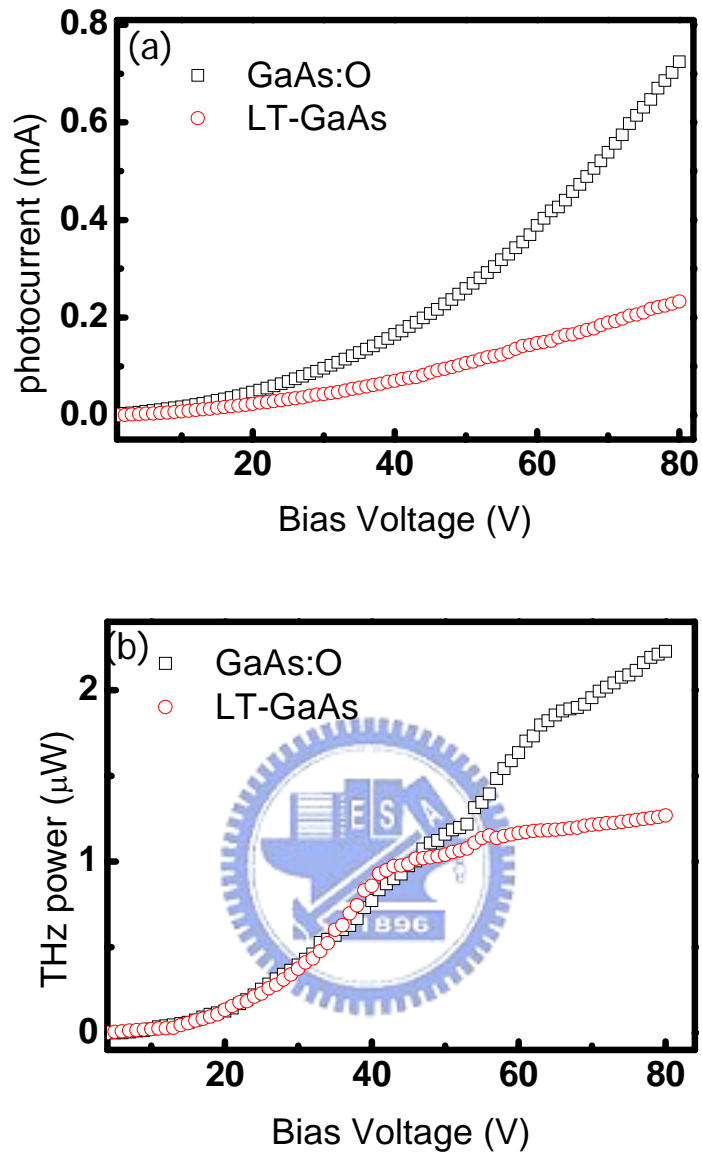
Figure 4.2-2 (a) photocurrent-bias voltage curve (b) THz power-bias voltage

curve of GaAs:O and LT-GaAs fabricated with the same dipole antenna

4.2-3 Analysis and Discussion

Figure 4.2-3 (a) shows the bias voltage dependence of the photocurrent measured for our photoconductive antennas using a constant pump power of 180mW which are 90mW for each other. According to the result, we observe that the photocurrent ratio of GaAs:O divide to LT-GaAs are increasing when bias is

more than 20V, The bias voltage below 20V are not increasing due to non-uniform electric field and low signal-noise ratio. And according to the CW theory, the carrier density is proportional the carrier lifetime ($n \propto \tau_e$), electron drift velocity is proportional the mobility at low electric field ($v \propto \mu_e$) and DC photocurrent is proportional to the carrier lifetime multiple mobility ($I_{ph}^{DC} = e\tau_e\mu_e$), so the mobility of GaAs:O is between 2.5 and 3.75 times to LT-GaAs.
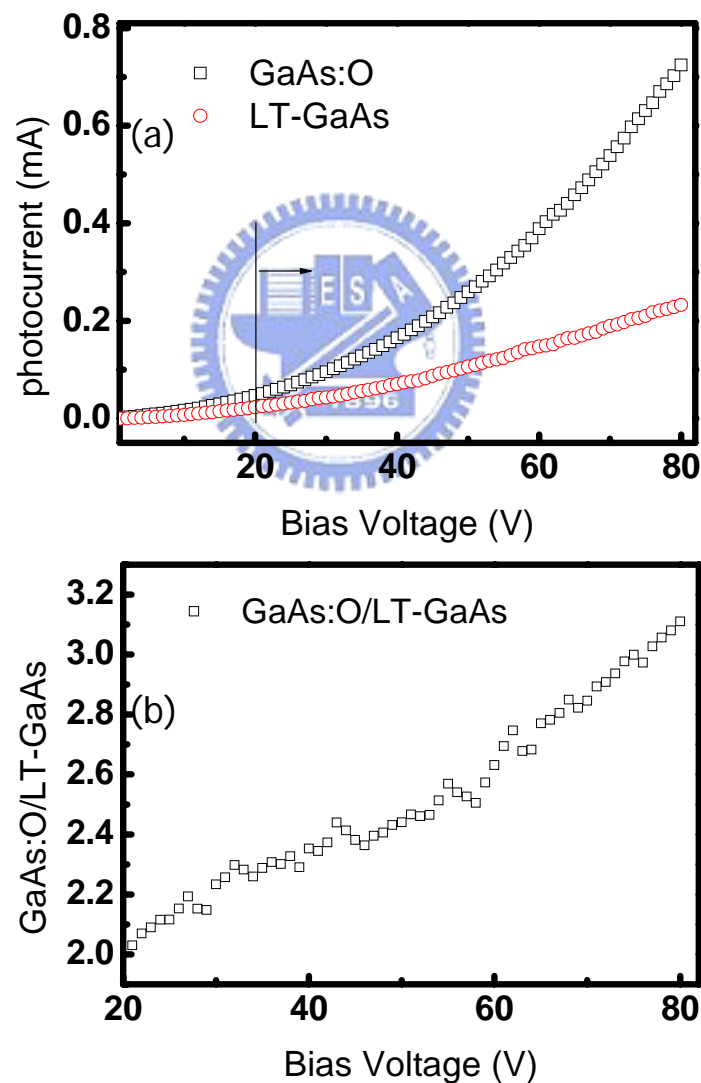
Figure 4.2-3 (a) photocurrent-bias voltage curve of both materials (b) the photocurrent ratio of GaAs:O divide to LT-GaAs

Figrue 4.2-4 (a) (b) (c) (d) show the DC photocurrent-electric field curve of GaAs:N GaAs:O and LT-GaAs. We observe the increase of onset voltage for quadratic behavior in the I-V curve corresponds to a consistent reduction of saturation in the P-I curve[48]. It means that the efficient of generation THz power with the same photocurrent are different when we implant different dosage density, due to different number of impact ion defects. The absence of additional very large defects (precipitates) which reduce the electron mobility may deteriorate the increase of carrier lifetime with voltage.
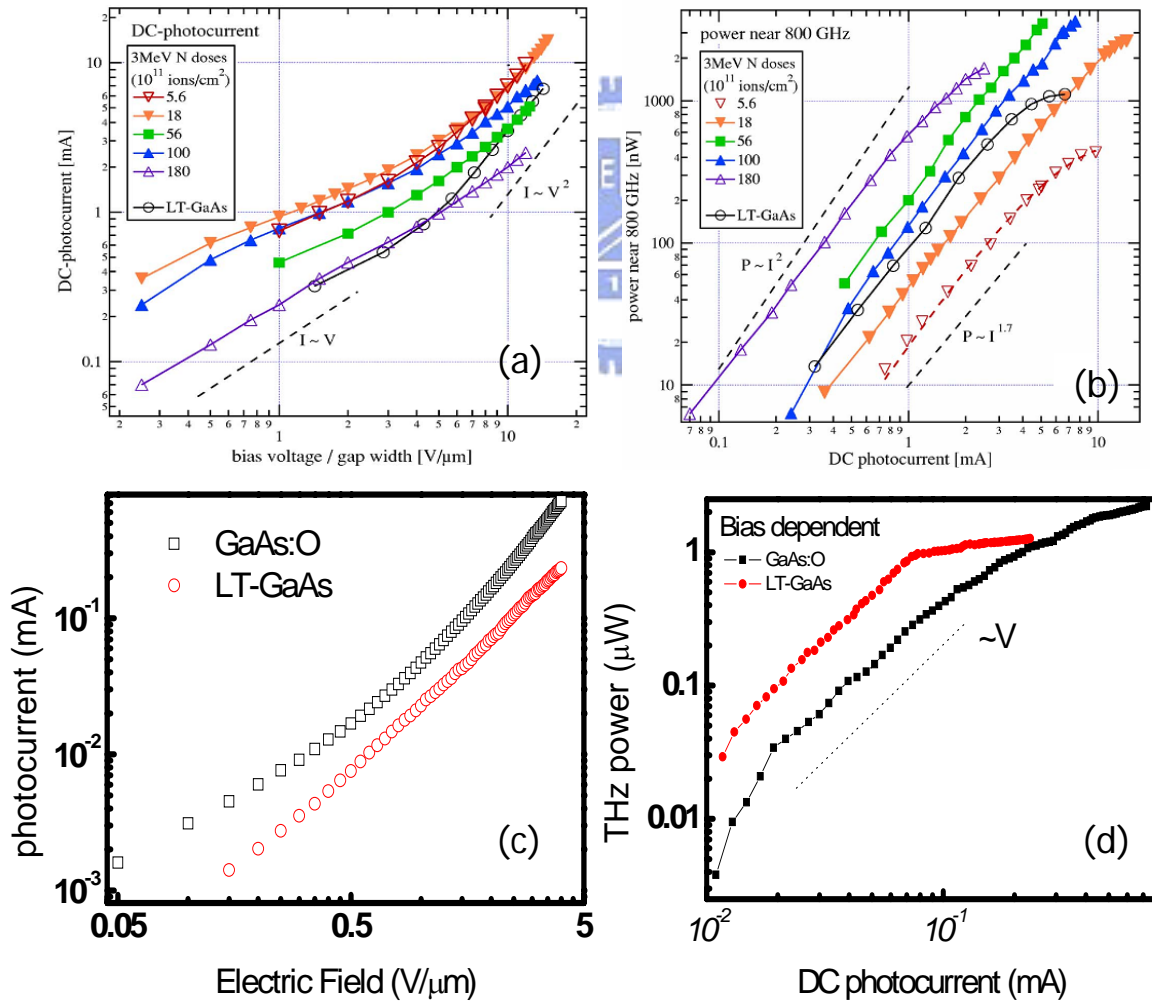
Figure 4.2-4 (a) Different dosage density of GaAs:N and LT-GaAs[48](c)

GaAs:O and LT-GaAs DC photocurrent-electric field curve (b)

Different dosage density of GaAs:N and LT-GaAs[48] (d) GaAs:O

and LT-GaAs THz power-DC photocurrent curve

In figure 4.2-5, we observe that THz power of LT-GaAs is saturated by the pump power. The reason of the LT-GaAs saturation is due to radiation field screening. Note that at low optical intensities the values of THz power is linear with optical pump that is the inverse of photoconductance and is greater than load impedance, when the optical intensities increase, the inverse of photoconductance has the same order to load impedance, THz power would respond nonlinear with optical pump power. But we didn't observe saturated effect occurred at GaAs:O, we attribute to higher conductivity compared to LT-GaAs
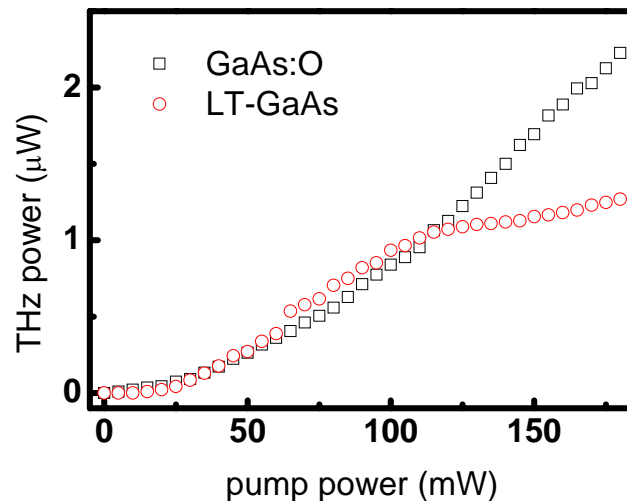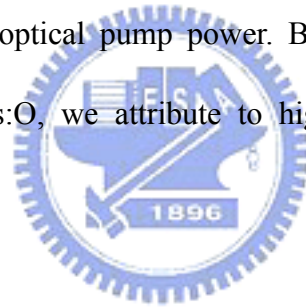
Figure 4.2-5 CW THz power-optical pump power for both materials.

In figure 4.2-6 (a) we observe that photocurrent are super-linear behavior on both materials. The reason that photocurrent has quadratic increasing is due to carrier life time increasing with voltage and that would increase the photoconductance and, consequently, the photocurrent. And under radiation field screening and carrier life time increasing we observe that GaAs:O has slightly saturated. Other effects such as impact ionization may play a role as well.
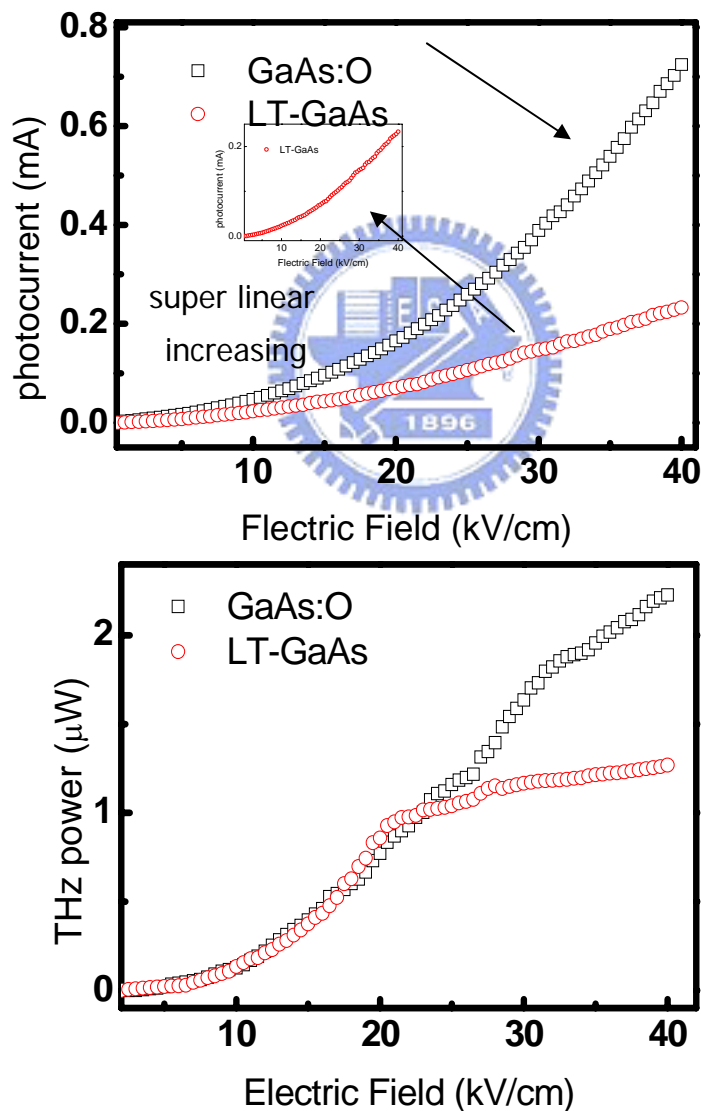
Figure 4.2-6 (a) photocurrent-electric field curve (b) THz power-electric field curve.

In figure 4.2-7 show that the spectrum of GaAs:O and LT-GaAs measured by CW heterodyne system. We calculate the resonant frequency the theory value is 0.34THz and our measurement value is 0.36THz. The bandwidth of both materials is about 1THz. They are identical to the value that we measured by THz-TDS system.
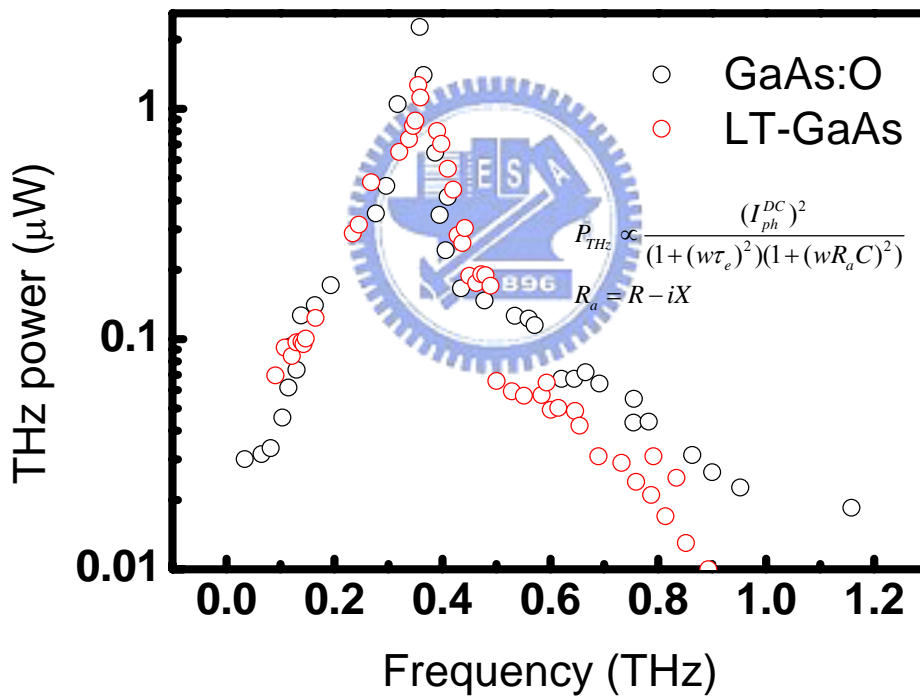
Figure 4.2-7 THz spectrum of both materials measured by CW heterodyne system

Chapter 5 Conclusion

In the last chapter, we conclude the results of emission properties and list some future works about oxygen-ion-implanted GaAs PC antennas.

5.1 Summary

We have demonstrated that the THz radiation generated from oxygen ion-implanted GaAs and LT-GaAs with dipole antenna structure under pulsed and CW mode. In our studies, we compared the emission properties of the LT-GaAs and GaAs implanted with oxygen multi-implants dosage concentrations 2.5×10^{13} ions/cm^2 （$500\ keV\ \&\ 800\ keV$）, 4×10^{13} ions/cm^2 （$1200\ keV$） and annealing temperature（$550℃$ for 60s).

From the result of electric measurement, oxygen-ion-implanted GaAs has higher increasing ratio when we bias at higher voltage, although oxygen-ion-implanted GaAs has higher dark current than low temperature grown GaAs.

From the result of THz radiation characteristics, the pulse THz peak power of oxygen ion implanted GaAs is 5.2mW, and that of the LT-GaAs is 3.6mW. It's almost 1.5 times the LT-GaAs. And we also measure the highest CW THz power of oxygen ion implanted GaAs is 2.268μW and for low temperature grown GaAs is 1.268μW. It's about 1.8 times the low temperature grown GaAs. The oxygen ion implanted GaAs has higher THz power both in pulse and CW mode and there

is no saturation effect in both pulse and CW mode. But low temperature grown GaAs has saturation effect in CW mode in our experiment. We also measurement the frequency bandwidth of both materials, the bandwidth of both materials are 1THz measured by pulse (TDS) and CW (photomixing). The results show that this kind of material is suitable for high power under both pumping sources THz radiation generation.

5.2 Future work

We have successfully demonstrated the THz radiation characteristics of two different materials (oxygen-ion-implanted and LT-GaAs) in pulse and CW mode. For the laser sources, we can replace our system to an external-cavity dual-wavelength laser diode. Because of the common-mode rejection effect and less mode-hopping the linewidth of beating frequency will become smaller than using two independent laser diodes. According to the recent study, they use interdigitated-fingner antenna structure to enhance CW THz power and optimize their fabricated conditions. And also traveling-wave structure could be used to maintain the bandwidth. So we can improve our emitters by optimizing the conditions of implant dosage and annealing temperature for high frequency purpose, or we can try to adopt other antenna structures to increase the bandwidth.

References

[01] Matthew C. beard, Gordon M. Turner, and Charles A. Schmuttenmaer, "Terahertz Spectroscopy" J. Phys. CHem. B, **Vol.106**, pp. 7146-7159, June. (2002)

[02] S. Mickan, D. Abbott, J. Munch, X. C. Zhang, T. can Doorn, "Analysis of system trade-offs for terahertz imaging" Microelectronics Journal, **Vol.31**, pp. 503-514,(2000)

[03] Sang-Gyu Park, M. R. Melloch, and A. M. Weiner, "Comparison of terahertz waveforms measured by electro-optic and photoconductive sampling" Appl. Phys Lett. **Vol.73**, pp. 3184-3186,(1998)

[04] B.B Hu, M. C. Nuss, "Imaging with terahertz waves", Opt. Lett. **20,** 1716 (1955)

[05] R.M. Woodward, V.P. Wallace, R.J. Pye, B.E. Cole, D.D. Arnone, E. Lin-field, M. Pepper,"Terahertz pulse imaging of ex vivo basal cell carcinoma, J. Invest, Derm." **73**, 120 (2003) 332

[06] Justin T. Darrow, Xi-Cheng Zhang, David H. Austion, Jeffrey D Morse," Saturation properties of large aperture photoconducting antennas" IEEE J. Quantum electron, **Vol.28**, no.6, pp.1607-1616,(1992)

[07] Masahiko Tani, Ping Gu, and Masaharu Hyodo et al. "Generation of coherent terahertz radiation by photomixing of dual-mode lasers", Optical and Quantum Electronics, Vol. **32,** pp. 503-520,(2000)

[08] M. Hyodo, M. Tani, S. Matsuura et al. "Generation of millimeter-wave radiation using a dual-longitudinal-mode microchip laser," Elec. Letts. Vol **32**, No. 17, pp1589-1591,(1996)

[09] S. Pajarola, G. Guekos, P. Nizzola et al. "Dual-polarization external-cavity diode laser transmitter for fiber-optic antenna remote feeding," IEEE Trans. Microwave Theory. , Vol47, No 7, pp. 1234-1240, (1999)

[10] K.A. McIntosh, E. R. Brwon, K. B. Nichols et al, "Terahertz photomixing with diode lasers in low-temperature-grown GaAs," Appl. Phys. Lett. , Vol **67** No. 17, pp. 2524-2526, (1999)

[11] Shuji Matsuura, Masahiko Tani, and Kiyomi Sakai, "Generation of coherent terahertz radiation by photomixing in dipole photoconductive antenna," Appl. Phys. Lett. , Vol. **70,** No. 5, pp. 559-561, (1997)

[12] D. H. Martin, and E. Puplett, "polarized interferometric spectrometry for the millimeter and submillimeter spectrum" Infrared Physics, **Vol.10**, pp. 105-109, (1969)

[13] O. Morikawa, M. Tonouchi, and M. Hangyo, "sub-THz spectroscopic system using a multimode laser diode and photoconductive antenna" Appl. Phys. Lett., **Vol.75**, No. 24, pp. 3772-3774,(1999)

[14] S. kono, M. Tani and K. Sakai, "Coherent Detection of mid-infrared radiation up to 60THz with an LT-GaAs photoconductive antenna" IEE, Proc-optoelectron, **Vol.149**, No. 3, pp. 105-109, (2002)

[15] Sang-Gyu Park, Michael R. Melloch, and Andrew M. Weiner, "Analysis of Terahertz Waveforms Measured by Photoconductive and electrooptic sampling" IEEE J. Quantum Electronics. **Vol.35**, No. 5, pp. 810-819,(1999)

[16] S Kono, Masahiko Tani, and Kiyomi Sakai, "Ultrabroadband photoconductive detection: comparison with free space electro optic sampling" Appl. Phys. Lett., **Vol.79**, No. 7, pp. 898-900, (2001)

[17] Sang-Gyu Park, M. R. Melloch, and A. M. Weiner, "Comparison photoconductive sampling" Appl. Phys Lett., **Vol.73**, pp. 3184-3186,(1998)

[18] Smith. F.W. Smith, F. W.; Le, H. Q.; Diadiuk, V.; Hollis, M. A.; Calawa, A. R.; Gupta, S.; Frankel, M.; Dykaar, D.R., "Picosecond GaAs-based photoconductive optoelectronic detectors." Appl. Phys. Lett. **Vol.54**, 890 (1989)

[19] M. Tani, K. Sakai, and H. Mimura, "Ultrafast Photoconductive Detectors

Based on Semi-Insulating GaAs and InP" Jpn. J. Appl. Phys., Part2, **Vol.36**, L1175 (1997)

[20] D. C. Look," Molecular beam epitaxial GaAs grown at low temperatures" Thin Solid Films 231, 61 (1993)

[21] C. Ludwig and J. Kuhl, "Studies of the temporal and spectral shape of terahertz pulses generated from photoconducting switches."Appl. Phys. Lett. **Vol.69**, 1194,(1996)

[22] S. Kono, M. Tani, And K. SaKai, "Ultrabroadband photocnductive detection: comparison with free-space electro-optic sampling" Appl. Phys. Lett., **Vol.79**, No.7, pp. 898-900, (2001)

[23] A. Claverie, F. Namavar, and Z. Lilorntal-Weber, "Formation of As precipitates in GaAs by ion implantation and thermal annealing."Appl. Phys. Lett. **Vol.62**, 1271,(1993)

[24] Liu T-A, Tani M and Pan C-L "THz radiation emission properties of multienergy arsenic-ion-implanted GaAs and semi-insulating GaAs based photoconductive antennas" J. Appl. Phys. **Vol.93**, 2996,(2003)

[25] Lin G-R, and Pan C-L "Characterization of optically excited terahertz radiation from arsenic-ion-implanted GaAs" Appl. Phys B **Vol.72**, 151,(2001)

[26] Lloyd-Hughes J, Castro-Camus E, fraser M D, Jagadish C and Johonston M B,"Carrier dynamics in ion-implanted GaAs studied by simulation and observation of terahertz emission", Phys. Rev. B 70 235330,(2004)

[27] Liu T-A, Tani M, Nakajima M,Hangyo M and Pan C-L "Ultrabroadband terahertz field detection by photoconductive antennas based on multi-energy arsenic-ion-implanted GaAs and semi-insulating GaAs." Appl. Phys. Lett. **Vol.83**, 1322,(2003)

[28] M. Lambsdorff, J. Kuhl, J, Rosenzweig, A. Axmann, and Jo. Schneider, "Subpicosecond carrier lifetimes in radiation-damaged GaAs."Appl. Phys. Let. **Vol.58**, 1881 (1991)

[29] M. J. Lederer, B. Luther-Davies, H. H. Tan, C. Jagadish, M. Haiml, U. Seifner,

and U. Keller, "Nonlinear optical absorption and temporal response of arsenic-and oxygen-implanted GaAs." Appl. Phys. Let. **Vol.74**, 1993 (1999)

[30] B. Salem, D. Morris, V. Aimez, J Veerens, J Beauvais and D Houde."Pulsed photoconductive antenna terahertz sources made on ion-implanted GaAs substrates" J. Phys.: Condens. Matter 17 7327-7333 (2005)

[31] M. Mikulics, E. A. Michael, M. Marso, M. Lepsa, A. van der Hart, and H. Lüth, A. Dewald, S. Stanček and M. Mozolik, P. Kordoš, "Traveling-wave photomixers fabrication on high energy nitrogen-ion-implanted GaAs", Appl. Phys. Lett. **Vol.89**, 071103, (2006)

[32] B.Salem, D.Morris, Y.Salissou, V.Aimez and S.Charlebois, M.Chicoine, F. Schiettekatte, "Terahertz emission properties of arsenic and oxygen ion-implanted GaAs based photoconductive pulsed sources" J.Vac.Sci. Technol. A 24(3), pp.774-777,(2006)

[33] B.Salem, D.Morris, V.Aimez, J Beauvais and D Houde, "Improved characteristics of a terahertz set-up built with an emitter and a detector made on proton-bombarded GaAs photoconductive materials" Semicond. Sci. Technol. **Vol.21**, 283-286,(2006)

[34] P.K. Benicewicz, J.P. Roberts, and A.J. Taylor, "Scaling of terahertz radiation from large-aperture biased photoconductors," J. Opt. Soc. Am. B, **Vol.11**, pp. 2533-2546, (1994)

[35] Davi K. Cheng, "Field and Wave Electromagnetics", 2nd Ed., Addison-Wesley. (1989)

[36] Justim T.Darrow, Xi Cheng Zhang, David H. Auston, Fellow, IEEE and Jeffrey D. Morse, "Saturation Properties of Large-Aperture Photoconducting Antennas" IEEE Journal of Quantum electronics, **Vol.28**, pp. 1607-1616, (1992)

[37] Zhisheng Piao, "Carrier Dynamics and Terahertz radiation in Photoconductive Antennas," Jpn. J. Appl. Phys., **Vol.39**, pp.96-100, (2000)

[38] P. Uhd Jepsn, R. H. Jacobsen, and S. R. Keiding, "Gereration and detection of terahertz pulses from biased semiconductor antennas," J. Opt. Soc. Am. B,

Vol.13, pp. 2424-2436, (1996)

[39] M. Tani, S. Matsuura, K. Sakai and S. Nakashima, "Emission characteristics of photoconductive antennas based on LT-GaAs and SI GaAs" Appl. Opt., **Vol.36**, No.30, pp. 7853-7859, Oct. (1997)

[40] S. Verghese, K. A. McIntosh, and E. R. Brown," Highly Tunable Fiber-coupled photomixers with coherent THz output power", IEEE Trans. Microwave Theory Tech. 45, 1301 (1997)

[41] A. W. Jackson, Ph.D. thesis, University of California at Santa Barbara (1999)

[42] J. C. G. Lesurf. "Millimetre-wave optics, devices and systems." Adam Hilger, January (1990)

[43] P. K. Benicewicz, J. P. Roberts, and A.J. Taylor," Scaling of Terahertz radiation form large aperture biased photoconductors ", J. Opt. Soc. Am. B 11, 2533 (1994)

[44] T. Darrow, X.-C. Zhang, and D.H. Auston, "Power scaling of large-aperture photoconducting antennas." Appl. Phys. Lett. **Vol.58**, 25 (1991)

[45] A. W. Sarto and B. J. Van Zeghbroeck," Photocurrents in a metal-semiconductor-metal photodector", IEEE J. Quantum Electron. **33, 2188** (1997)

[46] N. Zamdmer, Qing Hu, K. A. McIntosh, and S. Verghese,"Increase in response time of low-temperature-grown GaAs photoconductive switches at high voltage bias, Appl. Phys. Lett. **75,** 2313 (1999)

[47] I. Camara Mayorga, E.A. Michael, A. Schmitz, P. Van der Wal, and R. Gusten,"Terahertz photomixing in high energy oxygen- and nitrogen-ion-implanted GaAs", Appl. Phys. Lett., **91**, 031107 (2007)

[48] E. A. Michael, I. Camara Mayorga, and R. Gusten," Terahertz continous-wave large-area traveling-wave photomixers on high-energy low-dose ion-implanted GaAs", Appl. Phys. Lett. **90**, 171109 (2007)